

1 **Disruption of *Cdh23* exon 68 splicing leads to progressive hearing loss**
2 **in mice by affecting tip-link stability**

3 Nana Li^{a,1}, Shuang Liu^{b,1}, Dange Zhao^{c,1}, Haibo Du^a, Yuehui Xi^a, Xiaoxi Wei^c,
4 Qingling Liu^b, Ulrich Müller^d, Qing Lu^{c,2}, Wei Xiong^{b,2}, Zhigang Xu^{a,c,2}

5 ^aShandong Provincial Key Laboratory of Animal Cells and Developmental Biology
6 and Key Laboratory for Experimental Teratology of the Ministry of Education, School
7 of Life Sciences, Shandong University, Qingdao, Shandong 266237, China

8 ^bChinese Institute for Brain Research, Beijing 102206, China

9 ^cKey Laboratory for the Genetics of Developmental and Neuropsychiatric Disorders,
10 Ministry of Education, Bio-X Institutes, Shanghai Jiao Tong University, Shanghai
11 200030, China.

12 ^dThe Solomon H. Snyder Department of Neuroscience, Johns Hopkins University
13 School of Medicine, Baltimore, MD 21205, USA

14 ^eShandong Provincial Collaborative Innovation Center of Cell Biology, Shandong
15 Normal University, Jinan, Shandong 250014, China

16 ¹Contributed equally to this work

17 ²Corresponding author: xuzg@sdu.edu.cn (Zhigang Xu); wei_xiong@cibr.ac.cn (Wei
18 Xiong); luqing67@sjtu.edu.cn (Qing Lu)

19

20 **Classification:** Biological Sciences/Neuroscience

21 **Keywords:** CDH23; alternative splicing; hair cells; tip links; mechano-electrical
22 transduction

23 **Abstract**

24 Inner ear hair cells are characterized by the F-actin-based stereocilia that are arranged
25 into a staircase-like pattern on the apical surface of each hair cell. The tips of
26 shorter-row stereocilia are connected with the shafts of their neighboring taller-row
27 stereocilia through extracellular links named tip links, which are required for
28 mechano-electrical transduction (MET) in hair cells. Cadherin 23 (CDH23) forms the
29 upper part of tip links, and its cytoplasmic tail is inserted into the so-called upper
30 tip-link density (UTLD) that contains other proteins such as harmonin. *Cdh23* gene
31 contains 69 exons, and exon 68 is subjected to inner ear-specific alternative splicing.
32 In the present work, we show that the *Cdh23(+68)* transcript is predominantly
33 expressed in cochlear hair cells; however, deletion of *Cdh23* exon 68 does not affect
34 tip link formation in mice. Further examination revealed that the stability of tip links
35 is compromised by *Cdh23* exon 68 deletion, and *Cdh23* exon 68 knockout mice suffer
36 from progressive and noise-induced hearing loss. Moreover, we show that the
37 cytoplasmic tail of CDH23(+68) but not CDH23(-68) is engaged in phase
38 separation-mediated condensate formation together with harmonin. In conclusion, our
39 work suggests that alternative splicing of *Cdh23* exon 68 is necessary for the stability
40 of tip links through regulating condensate formation of UTLD components.

41

42

43

44

45 **Significance statement**

46 Mechano-electrical transduction (MET) in inner ear hair cells requires tip links, which
47 are formed by single-transmembrane proteins cadherin 23 (CDH23) and
48 protocadherin 15 (PCDH15). The *Cdh23* gene is subjected to alternative splicing and
49 exon 68 is only expressed in the inner ear. The physiological significance of this
50 tissue-specific splicing of *Cdh23* exon 68 has remained elusive. Here we show that
51 *Cdh23* exon 68 is necessary for maintaining tip-link stability, and mice with a *Cdh23*
52 exon 68 deletion suffer from progressive and noise-induced hearing loss. We also
53 provide evidence that exon 68 regulates CDH23 homodimerization and condensate
54 formation with harmonin, a cytoplasmic binding partner for CDH23 that is
55 concentrated at the tip-link insertion point near CDH23.

56

57

58

59

60

61

62

63

64

65

66

67 **Introduction**

68 As the mechanosensitive receptor cells in the inner ear, hair cells are characterized by
69 their hair bundles on the apical cell surface. The hair bundle of each hair cell consists
70 of one tubulin-based kinocilium and dozens of F-actin-based stereocilia (1). The
71 kinocilium plays an important role in hair bundle development, but is not necessary
72 for mechano-electrical transduction (MET) (2, 3). The kinocilium is lost in mature
73 cochlear hair cells, whereas it persists in mature vestibular hair cells (1). On the other
74 hand, the stereocilia are indispensable for MET, organized into rows of increasing
75 height forming a staircase-like pattern in each hair cell (2). Various types of
76 extracellular links provide connections between individual stereocilia as well as
77 between the kinocilium and its neighboring tallest-row stereocilia in each hair cell.
78 These linkages include tip links, horizontal top-connectors, lateral links, ankle links,
79 and kinociliary links (4-6). Tip links connect the tips of shorter-row stereocilia with the
80 shafts of neighboring taller-row stereocilia and are important for MET (4, 6, 7). When
81 mechanical force deflects stereocilia towards the taller edge of the hair bundle, the
82 tension in tip links is thought to increase, which in turn affects the open probability of
83 MET channels localized near the lower end of tip links, resulting in the influx of
84 cations into hair cells (2, 8, 9).

85 Two single-transmembrane cadherins, cadherin 23 (CDH23) and protocadherin 15
86 (PCDH15), have been shown to be essential components of lateral links, kinociliary
87 links, and tip links (10-16). In tip links, CDH23 and PCDH15 form cis-homodimers
88 through lateral interaction and trans-interact with each other via their N-terminal

89 extracellular cadherin (EC) domains, forming the upper and lower part of tip links,
90 respectively (12) (Fig. 1A). Mutations of *CDH23* and *PCDH15* gene cause syndromic
91 and non-syndromic hearing loss in human (17-20). Consistently, mutations in the
92 *Cdh23* and *Pcdh15* gene in mice lead to deficits in the stereocilia and tip links, as well
93 as to hearing loss (21-23). The upper and lower ends of tip links are anchored to the
94 stereociliary membrane in electron-dense plaques referred to as upper tip-link density
95 (UTLD) and lower tip-link density (LTLD), respectively (5, 24) (Fig. 1A).
96 Immunolocalization studies revealed that UTLD components include Myosin VIIA
97 (MYO7A), SANS, and harmonin in addition to the cytoplasmic tail of CDH23 (25,
98 26). Recently, it was suggested that MYO7A, SANS, and harmonin may form the
99 UTLD via phase separation (27).

100 Transcription from different transcriptional start sites produces three main CDH23
101 isoforms, namely CDH23-V1 and CDH23-V2 with 27 and 7 extracellular EC domains,
102 respectively, and CDH23-V3, which is a cytosolic protein (13) (Fig. 1B). Moreover,
103 the *Cdh23* gene contains 69 exons, and exon 68 is subjected to alternative splicing
104 thus gives rise to two CDH23 isoforms, CDH23(+68) and CDH23(-68) (10, 13, 28)
105 (Fig. 1B). *Cdh23* is expressed in multiple tissues, whereas exon 68 inclusion has so
106 far only been detected in the inner ear (29). Exon 68 is 105 base pairs (bp) long,
107 encoding a peptide of 35 amino acids in the cytoplasmic tail of CDH23, which
108 regulates the interaction of CDH23 with harmonin (28). Immunoreactivity with an
109 antibody against this exon 68-encoded peptide specifically localizes to the stereocilia,
110 raising the possibility that CDH23(+68) might be the CDH23 isoform that forms tip

111 links (10). However, the physiological significance of *Cdh23* exon 68 alternative
112 splicing is unknown.

113 To explore the biological role of exon 68 splicing, we established knockout mice
114 with *Cdh23* exon 68 deleted. Unexpectedly, tip links still form and function in young
115 knockout mice, suggesting that CDH23(+68) is not essential for tip link formation.
116 However, knockout of exon 68 leads to loss of tip links and degeneration of
117 shorter-row mechanosensory stereocilia in aged mice or mice exposed to noise,
118 suggesting that CDH23(+68) is required for the stability of tip links. Further
119 investigations revealed that the exon 68-encoded peptide is necessary for dimerization
120 of CDH23 as well as condensate formation with harmonin.

121

122 **Results**

123 **CDH23 isoforms show different expression patterns in the mouse cochlea.** We
124 first examined the expression pattern of *Cdh23(+68)* and *Cdh23(-68)* transcripts in
125 mouse cochlea by performing reverse transcription-polymerase chain reaction
126 (RT-PCR). Both transcripts were readily detected in the sensory epithelium and spiral
127 ganglion at postnatal day 0 (P0) (Fig. 1C). However, at P15 and P45, *Cdh23(+68)*
128 was predominantly expressed in the sensory epithelium, whereas *Cdh23(-68)* was
129 predominantly expressed in the spiral ganglion (Fig. 1C). We then isolated cochlear
130 hair cells from *Atoh1*-GFP transgenic mice to examine *Cdh23* expression by RT-PCR.
131 The results showed that *Cdh23(+68)* was predominantly expressed in P0 and P15
132 cochlear hair cells (Fig. 1D). Therefore, our present data are consistent with the

133 hypothesis that CDH23(+68) is the main CDH23 isoform that forms tip links in
134 cochlear hair cells.

135 We then employed injectoporation experiments to examine the localization of
136 different CDH23 isoforms in cochlear hair cells. Expression vectors for different
137 CDH23 isoforms with an HA tag at their C-termini were introduced into cochlear hair
138 cells. Immunostaining with anti-HA antibody revealed that for the longest CDH23
139 isoform (V1), both CDH23(+68) and CDH23(-68) were localized to the stereocilia as
140 well as in the cell body (Fig. 1E). For the second longest isoform (V2), both
141 CDH23(+68) and CDH23(-68) were only detected in the cell body (Fig. 1E). Similar
142 cytoplasmic localization was observed for the shortest isoform (V3) (Fig. 1E). As
143 mentioned above, different from V1 and V2 isoforms that contain transmembrane
144 segments, CDH23-V3 is a short, cytosolic protein, and adding a tag to its C terminus
145 might affect its subcellular localization. Therefore, we added the HA tag to the N
146 terminus of CDH23-V3, which was detected in the stereocilia as well as cell body in
147 injectoprated hair cells (Fig. 1E). Together, our present data demonstrate that V1 and
148 V3 isoforms of CDH23 can localize to the stereocilia.

149

150 **Deletion of *Cdh23* exon 68 leads to hearing loss but not balance deficits.** To
151 investigate the function of *Cdh23* exon 68 splicing, we established knockout mice
152 with *Cdh23* exon 68 deleted using the clustered regularly interspaced short
153 palindromic repeat (CRISPR)/CRISPR-associated protein 9 (Cas9) genome editing
154 technique (Fig. 2A). Sanger sequencing confirmed that a deletion of 218 bp including

155 the entire exon 68 was introduced into the genome of the knockout mice (Fig. S1A
156 and B). The obtained F0 mouse was in a C57BL/6 and CBA/CaJ mixed background,
157 which was then crossed back to CBA/CaJ wild-type mice to generate heterozygous
158 and eventually homozygous knockout mice. C57BL/6 but not CBA/CaJ mice carry
159 the hypomorphic *Cdh23*^{753A} allele that causes progressive hearing loss (30). Sanger
160 sequencing revealed that the heterozygous and homozygous knockout mice only
161 carried the *Cdh23*^{753G} allele (Fig. S1C), therefore excluding the potential interference
162 of the *Cdh23*^{753A} site on our following analysis.

163 RT-PCR results confirmed that *Cdh23(+68)* was no longer expressed in the cochlea
164 of the knockout mice (Fig. 2B). Auditory brainstem response (ABR) measurements to
165 click stimuli showed that there was a nearly 30 dB hearing threshold elevation in P18
166 *Cdh23*^{Δ68/Δ68} mice compared to *Cdh23*^{+/Δ68} mice (Fig. 2C and Fig. S2A). The hearing
167 threshold elevation was more pronounced in aged knockout mice (Fig. 2C and Fig.
168 S2A). ABR measurements to pure tone stimuli revealed that hearing thresholds were
169 elevated in *Cdh23*^{Δ68/Δ68} mice at P18 and 4 months of age at all frequencies examined
170 (Fig. 2D, Fig. S2B and S2C). The ABR thresholds of *Cdh23*^{+/Δ68} mice were
171 indistinguishable from wild-type mice (Fig. S2A - S2C). Therefore, *Cdh23*^{+/Δ68} mice
172 were used as control in the subsequent experiments. To examine outer hair cell (OHC)
173 function in *Cdh23*^{Δ68/Δ68} mice, we measured distortion product otoacoustic emissions
174 (DPOAEs). DPOAE thresholds in *Cdh23*^{Δ68/Δ68} mice at P30 were significantly
175 elevated compared to *Cdh23*^{+/Δ68} mice, suggesting that OHC function was
176 compromised by *Cdh23* exon 68 deletion (Fig. 2E).

177 RT-PCR results also confirmed that *Cdh23(+68)* was no longer expressed in the
178 vestibule of knockout mice (Fig. S3A). We evaluated the vestibular function of
179 *Cdh23 Δ^{68}/Δ^{68}* mice by performing rotarod test, swimming test, tail hanging test,
180 stereotyped circling movement test, retropulsion test, and head bobbing test.
181 *Cdh23^{v2J/v2J}* mice were included as positive control, which have been shown to
182 possess balance deficits (22). *Cdh23^{v2J/v2J}* mice indeed showed severe balance deficits,
183 whereas vestibular function of *Cdh23 Δ^{68}/Δ^{68}* mice was not significantly different from
184 *Cdh23⁺/ Δ^{68}* mice when examined at age of 7 months (Fig. 2F - K). Consistently,
185 phalloidin staining and scanning electron microscopy (SEM) suggested that hair
186 bundle morphology in vestibular hair cells was unaffected in 7-month-old
187 *Cdh23 Δ^{68}/Δ^{68}* mice (Fig. S3B - D'). Taken together, our data suggest that
188 *Cdh23 Δ^{68}/Δ^{68}* mice have hearing loss but preserved vestibular function.

189

190 **Deletion of *Cdh23* exon 68 does not affect tip link formation or MET function in**
191 **young mice.** CDH23 has been shown to be a component of tip links, lateral links, and
192 kinocilial links in developing hair cells (10, 13-16). In mature cochlear hair cells,
193 however, CDH23 is mainly present in tip links, as lateral links and kinocilial links are
194 transient structures that only exist in developing cochlear hair cells (6, 10, 12). We
195 therefore examined tip links in mature cochlear hair cells of *Cdh23* exon 68 knockout
196 mice, initially by analyzing the expression of CDH23 using immunohistochemistry
197 with a custom antibody that detects the CDH23(+68) and CDH23 (-68) cytoplasmic
198 tail. CDH23 was detected near the tip of stereocilia in control mice but not

199 *Cdh23*^{v2J/v2J} mice at P8, confirming the specificity of the antibody and the absence of
200 tip links in *Cdh23*^{v2J/v2J} mice (Fig. 3A and B). Stereociliary tip localization of CDH23
201 was also observed in P8 *Cdh23*^{Δ68/Δ68} mice, suggesting that tip link formation was
202 unaffected by *Cdh23* exon 68 deletion (Fig. 3A and B). Next, we carried out SEM
203 analysis to examine the shape of stereociliary tips. Beveled tips are thought to result
204 from tip-link-mediated tension and are therefore a proxy for the presence of tip links
205 (5, 7, 24, 31). We focused on the second-row stereocilia, whose relatively large
206 dimension facilitates measurement of tip shape. Beveled second-row stereociliary tips
207 were detected in the cochlear hair cells from P8 *Cdh23*^{Δ68/Δ68} and control mice, but
208 not in *Cdh23*^{v2J/v2J} mice, suggesting that tip link formation was not affected by *Cdh23*
209 exon 68 deletion (Fig. 3C and D). Lastly, we directly quantified the numbers of tip
210 links in SEM images. Tip link numbers were comparable in control mice and
211 *Cdh23*^{Δ68/Δ68} mutants (Fig. 3E and F).

212 Normal tip link formation suggests that MET function might be preserved in young
213 *Cdh23*^{Δ68/Δ68} mice. To test this hypothesis, FM1-43FX dye uptake experiments were
214 performed in mice of different genotypes. Up to P30, FM1-43FX dye uptake in
215 *Cdh23*^{Δ68/Δ68} hair cells was indistinguishable to that in control *Cdh23*^{+ /Δ68} hair cells
216 (Fig. 3G and H). We then recorded and quantified maximal MET currents by patch
217 clamping hair cells whose hair bundles were deflected with fluid-jet. An averaged
218 peak MET current of 697±39 pA was recorded from P6-P8 *Cdh23*^{Δ68/Δ68} OHCs,
219 which is comparable to the current from control *Cdh23*^{+ /Δ68} OHCs (701±21 pA) (Fig.
220 4A and B). We also analyzed MET current kinetics from P6-P8 OHCs in response to

221 10-ms bundle deflections ranging from -300 to 1000 nm using a stiff probe (Fig. 4C).
222 The activation and adaptation time constant of MET currents was not significantly
223 different between *Cdh23*^{Δ68/Δ68} and control *Cdh23*^{+ /Δ68} mice (Fig. 4C - F). Lastly, we
224 measured voltage-gated currents of OHCs, which again did not show any significant
225 difference between *Cdh23*^{Δ68/Δ68} and control *Cdh23*^{+ /Δ68} mice (Fig. 4G and H). We
226 conclude that MET function of cochlear hair cells was unaffected in young
227 *Cdh23*^{Δ68/Δ68} mice.

228

229 **Deletion of *Cdh23* exon 68 causes stereocilia degeneration and OHC loss in adult**
230 **mice.** ABR measurements revealed progressive hearing threshold elevation in
231 *Cdh23*^{Δ68/Δ68} mice (Fig. 2C). We then employed SEM to examine hair bundle
232 morphology in *Cdh23*^{Δ68/Δ68} mice at older ages. At one month of age, the morphology
233 of hair bundles in *Cdh23*^{Δ68/Δ68} mice appeared largely normal (Fig. 5A). However,
234 significant hair bundle loss was detected in 5-month-old *Cdh23*^{Δ68/Δ68} OHCs,
235 especially in the basal cochlear turn, which was further exaggerated in 8-month-old
236 *Cdh23*^{Δ68/Δ68} OHCs (Fig. 5A and B). High-magnification SEM showed that
237 degeneration of third-row stereocilia was detected in *Cdh23*^{Δ68/Δ68} OHCs at as early
238 as P14, with increasing degeneration at subsequent ages (Fig. 5C and D).
239 Degeneration of third-row stereocilia was also observed in inner hair cells (IHCs) of
240 *Cdh23*^{Δ68/Δ68} mice at P14 (Fig. 6A and B), albeit no complete hair bundle loss was
241 detected in *Cdh23*^{Δ68/Δ68} IHCs up to 8 months (Fig. 5A).

242 Immunostaining with an antibody against the hair cell marker MYO7A revealed

243 significant OHC loss in the basal cochlear turn of 5-month-old *Cdh23*^{Δ68/Δ68} mice
244 (Fig. S4A, B, and D). By 8 months of age, OHC loss becomes more severe and
245 extends to the apical cochlear turn in *Cdh23*^{Δ68/Δ68} mice (Fig. S4C and D).
246 Meanwhile, no significant IHC loss was detected in *Cdh23*^{Δ68/Δ68} mice at any time
247 points examined (Fig. S4A-C). Taken together, our data show that deletion of *Cdh23*
248 exon 68 leads to stereocilia degeneration and OHC loss in adult mice.

249

250 **Adult *Cdh23*^{Δ68/Δ68} mice show decreased tip-link numbers and compromised**
251 **MET.** Degeneration of third-row mechanosensitive stereocilia might result from loss
252 of tip links in adult *Cdh23*^{Δ68/Δ68} mice. High-magnification SEM was then employed
253 to examine beveled stereociliary tips and tip-link numbers in adult mice. Beveled
254 second-row stereociliary tips were less prominent in 5-month-old *Cdh23*^{Δ68/Δ68} IHCs
255 (Fig. 6C), and tip-link numbers were significantly reduced in 8-month-old
256 *Cdh23*^{Δ68/Δ68} OHCs and IHCs (Fig. 6D and E). Furthermore, the intensity of CDH23
257 immunoreactivity was decreased in 5-month-old *Cdh23*^{Δ68/Δ68} OHCs (Fig. 6F and G).
258 Finally, FM1-43FX uptake was also decreased in 5-month-old *Cdh23*^{Δ68/Δ68} cochlear
259 hair cells (Fig. 6H and I). Taken together, our data suggest that *Cdh23* exon 68
260 deletion affects the stability of tip links thus leading to tip-link loss as mice age,
261 which in turn is expected to compromise MET and lead to hearing loss.

262

263 **Deletion of *Cdh23* exon 68 contributes to noise-induced hearing loss.** Tip-link
264 stability is affected by noise exposure that causes hearing loss (32, 33). We wanted to

265 determine whether adult *Cdh23*^{Δ68/Δ68} mice were more vulnerable to acoustic trauma.
266 Exposure to a broadband noise of 2-20 kHz at 96 dB sound pressure level (SPL) for 2
267 hours caused a temporary threshold shift (TTS) in *Cdh23*^{+/-Δ68} mice, with normal ABR
268 thresholds restored 14 days later (Fig. 7A and B). The same noise exposure paradigm
269 led to greater, permanent threshold shift (PTS) in *Cdh23*^{Δ68/Δ68} mice (Fig. 7A and B).
270 Consistently, SEM revealed that noise exposure induces enhanced OHC hair bundle
271 loss in *Cdh23*^{Δ68/Δ68} mice at both 1 day and 14 days after noise exposure (Fig. 7C and
272 D). High-magnification SEM further revealed significant degeneration of third-row
273 stereocilia in *Cdh23*^{Δ68/Δ68} OHCs (Fig. 7E and F) and IHCs 14 days after exposure to
274 noise (Fig. 8A and B).

275 To our surprise, high-magnification SEM revealed that beveled second-row
276 stereociliary tips in *Cdh23*^{Δ68/Δ68} IHCs, similar to control *Cdh23*^{+/-Δ68} mice, were still
277 present after noise exposure (Fig. 8C). Similarly, direct examination of tip links using
278 SEM did not reveal a significant difference in tip-link numbers between *Cdh23*^{Δ68/Δ68}
279 and control *Cdh23*^{+/-Δ68} mice after noise exposure (Fig. 8D and E). Strikingly, CDH23
280 immunoreactivity was significantly decreased in *Cdh23*^{Δ68/Δ68} mice at 1 day and 14
281 days after noise exposure (Fig. 8F and G). In addition, FM1-43FX uptake was also
282 significantly decreased in *Cdh23*^{Δ68/Δ68} mice at 1 day and 14 days after noise
283 exposure, suggesting of compromised MET function (Fig. 8H and I). Taken together,
284 our data suggest that *Cdh23*^{Δ68/Δ68} mice are more vulnerable to acoustic trauma.

285

286 **Exon 68 of CDH23 affects harmonin condensate formation.** To gain insights into

287 the mechanisms by which *Cdh23* alternative splicing regulates tip-link stability, we
288 carried out biochemical experiments. It has been suggested that the exon 68-encoded
289 peptide induces dimerization of the cytoplasmic tail of CDH23 (34). Consistently,
290 yeast two-hybrid and co-immunoprecipitation (co-IP) results showed that the
291 cytoplasmic tail of CDH23(+68) but not CDH23(-68) mediates homo-dimerization
292 (Fig. 9A and B). Furthermore, co-sedimentation assays confirmed that the purified
293 cytoplasmic tail of CDH23(+68) was more enriched in the pellet fraction than the
294 cytoplasmic tail of CDH23(-68) (Fig. 9C).

295 The cytoplasmic tail of CDH23 interacts with harmonin, which has been suggested
296 to participate in UTLD formation via phase separation together with MYO7A and
297 SANS (27, 28, 35-37). We therefore determined whether *Cdh23* exon 68 splicing
298 affects condensate formation of CDH23 and harmonin. The longest harmonin isoform
299 (harmonin-b) contains a N-terminal domain (NTD), three PDZ domains, two
300 coiled-coil (CC) domains, and a proline, serine, and threonine-rich (PST) domain.
301 Harmonin binds to the cytoplasmic tail of CDH23 through its NTD and the second
302 PDZ domain (PDZ2) (25, 28, 35, 36). Therefore, we performed co-sedimentation
303 assays with the purified CDH23 cytoplasmic tail and harmonin NPDZ12 fragment
304 that contains the NTD and the first two PDZ domains. CDH23(+68) predominantly
305 co-sedimented with the harmonin NPDZ12 fragment (Fig. 9D). When the Cy3-labeled
306 CDH23(+68) cytoplasmic tail was mixed with Alexa 488-labeled harmonin NPDZ12
307 fragment, significant spherical droplets with enrichment of both proteins were
308 observed by fluorescence microscopy (Fig. 9E). Moreover, these droplets formed in a

309 dose-dependent manner (Fig. 9F). In contrast, the CDH23(-68) cytoplasmic tail barely
310 formed large droplets with the harmonin NPDZ12 fragment (Fig. 9E and 9F). We then
311 conducted fluorescence recovery after photobleaching (FRAP) assay to evaluate the
312 mobility of CDH23(+68) cytoplasmic tail within the droplets. Within eight minutes
313 after photobleaching, only 20-40% of the fluorescence signal recovered (Fig. 9G and
314 9H), suggesting that CDH23(+68) cytoplasmic tail forms solid-like condensates with
315 harmonin. Taken together, our results provide evidence that exon 68 of CDH23 plays
316 a role in the assembly of condensates involving harmonin.

317

318 **Discussion**

319 About the alternative splicing of *Cdh23* exon 68, two intriguing questions have
320 remained unanswered for many years. First, how is this inner ear-specific splicing
321 regulated? Second, what is the biological significance of this alternative splicing? Our
322 recent work provided the answer to the first question. Through cell-based screening,
323 we found that alternative splicing of *Cdh23* exon 68 is promoted by RBM24 and
324 RBM38, and inhibited by PTBP1 (38). Moreover, the inclusion of *Cdh23* exon 68 is
325 almost completely abolished in the cochlea of *Rbm24* knockout mice (39). Our
326 present work now provides insights into the answer to the second question. Our data
327 suggest that *Cdh23* exon 68 is important for maintaining the stability of tip links
328 through regulating UTLD formation.

329 Our RT-PCR results showed that *Cdh23(+68)* transcript is predominantly expressed
330 in postnatal cochlear hair cells, implying that CDH23(+68) but not CDH23(-68) is the

331 main CDH23 isoform that forms tip links in mature hair cells. Surprisingly, the
332 formation and function of tip links are largely unaffected in young mice with *Cdh23*
333 exon 68 deleted. Several lines of evidence support this conclusion. First, CDH23
334 immunoreactivity in the stereocilia is unaffected in young *Cdh23*^{Δ68/Δ68} mice. Second,
335 beveled stereociliary tips, an indicator of the presence of functional tip links, is
336 unaffected in young *Cdh23*^{Δ68/Δ68} mice. Third, tip links directly examined using SEM
337 is unaffected in young *Cdh23*^{Δ68/Δ68} mice. Fourth, *Cdh23* exon 68 deletion in young
338 mice does not affect FM1-43FX dye uptake, an indicator of functional integrity of
339 hair cells. Last, the electrophysiology results confirmed that *Cdh23* exon 68 deletion
340 does not affect MET in young mice. Together, our present data reveal that albeit
341 CDH23(+68) mainly forms tip links in native hair cells, CDH23(-68) could fulfill this
342 function when CDH23(+68) is absent.

343 However, the CDH23(-68)-mediated tip links are less stable than regular
344 CDH23(+68)-mediated tip links. It has been shown that tip links are sensitive to
345 environmental insults such as aging and noise (23, 32, 40). Our data reveal that the
346 number of tip links is significantly decreased in aged *Cdh23*^{Δ68/Δ68} mice. Moreover,
347 aged *Cdh23*^{Δ68/Δ68} mice show robust stereocilia degeneration and reduced FM1-43FX
348 dye uptake. Consistently, *Cdh23*^{Δ68/Δ68} mice manifest progressive hearing loss.
349 Therefore, our present data suggest that deletion of *Cdh23* exon 68 affects the stability
350 of tip links, and eventually contributes to progressive hearing loss. Inclusion of *Cdh23*
351 exon 68 happens in both the cochlea and vestibula. However, in contrast to auditory
352 system, no balance deficits could be detected in *Cdh23*^{Δ68/Δ68} mice up to 7 months of

353 age. Compared to cochlear stereocilia, vestibular stereocilia are subjected to less
354 intense daily stimuli, which might explain why tip links in vestibular hair cells are
355 more stable even when exon 68 is absent.

356 When subjected to noise stimuli that lead to TTS in control mice, *Cdh23*^{Δ68/Δ68}
357 mice manifest PTS with greater threshold elevation. Enhanced stereocilia
358 degeneration and reduced FM1-43FX dye uptake were also observed in noise-exposed
359 *Cdh23*^{Δ68/Δ68} mice. However, the number of tip links was unaffected when examined
360 1 day or 14 days after noise exposure. It has been suggested that tip links recover
361 within seconds to hours after disruption by Ca²⁺ chelation (41-43). It's tempting to
362 speculate that tip-link recovery might also happen quickly in a similar time scale after
363 noise exposure, which explains why we did not detect tip-link loss in noise-exposed
364 mice. Nevertheless, the temporary tip-link loss might lead to stereocilia degeneration,
365 which could not be restored easily and eventually contribute to the observed
366 noise-induced hearing loss. Consistent with this hypothesis, loss of tip links could
367 only be detected in adult *Cdh23*^{Δ68/Δ68} mice at rather late age.

368 Further investigation showed that the CDH23(+68) cytoplasmic tail is more prone
369 to dimerize and form condensates than the CDH23(-68) cytoplasmic tail. It has been
370 shown that the cytoplasmic tail of CDH23, as well as harmonin, MYO7A, and SANS
371 interact with each other and form a so-called UTLD protein complex at the upper
372 insertion site of tip links (5, 24-26). In line with this, harmonin, MYO7A, and SANS
373 form condensates via phase separation (27). Moreover, the CDH23(+68) cytoplasmic
374 tail and harmonin form large protein assemblies through multivalent interactions (34).

375 Our present data confirm that the cytoplasmic tail of CDH23(+68) but not
376 CDH23(-68) dimerize and form condensates together with harmonin, suggesting that
377 the CDH23(+68) cytoplasmic tail might contribute to the formation of the UTLD. Our
378 data also imply that the CDH23 short isoform (CDH23-V3) might play an important
379 role in this process. CDH23-V3(+68) can bind to CDH23-V1(+68), and therefore
380 might contribute to the formation of a large protein condensate near the upper end of
381 tip links through multivalent interactions with other UTLD components (Fig. S5).

382 Hearing threshold elevation was observed as early as P18 in *Cdh23*^{Δ68/Δ68} mice, by
383 which time stereocilia morphology was largely normal, and MET function revealed
384 by FM1-43FX uptake was also not significantly affected. Therefore, cochlear function
385 that does not involve tip links and even stereocilia might be compromised by *Cdh23*
386 exon 68 deletion. It has been shown that ribbon synapse numbers are significantly
387 reduced in aged C57BL/6N mice that carry the hypomorphic *Cdh23*^{753A} allele, and
388 repair of this mutation partially rescues the phenotype (44, 45). Further investigations
389 are warranted to fully understand the potential role of CDH23 in the synapse.

390 Our injectoporation results revealed that CDH23 V1 and V3 but not V2 isoforms
391 are localized to the stereocilia. The underlying mechanism of this differential
392 transport of CDH23 isoforms is not fully understood. The lower tip-link component,
393 PCDH15, has three different isoforms, namely PCDH15-CD1, -CD2, and -CD3,
394 which share common extracellular and transmembrane domains but differ in the
395 cytoplasmic tail (11). We and other groups have shown that Golgi-associated
396 chaperon protein PIST as well as unconventional myosins MYO3A, MYO3B, and

397 MYO7A might play important roles in the differential transport of PCDH15 isoforms
398 in a heterologous expression system (46, 47). Interestingly, we found that PIST also
399 binds to the cytoplasmic PDZ-binding-interface (PBI) of CDH23 and regulates its
400 membrane localization in a heterologous expression system (48). However,
401 considering that all CDH23 isoforms share similar cytoplasmic tails, it seems unlikely
402 that PIST or unconventional myosins differentially regulate the transport of CDH23
403 isoforms. Alternatively, CDH23's targeting to and/or retention in the stereocilia might
404 require interaction of the N-terminal EC domains of CDH23 with the N-terminal
405 PCDH15 EC domains (49). Therefore, it is tempting to speculate that CDH23-V2 was
406 not present in stereocilia because it lacks PCDH15-binding sites present in
407 CDH23-V1. Another possibility is that CDH23-V2 lacks a N-terminal signal peptide
408 and is therefore unable to target to the plasma membrane. CDH23-V3, as a small
409 soluble protein, might be transported to the stereocilia through binding to the
410 cytoplasmic tail of CDH23-V1.

411

412 **Materials and Methods**

413 Animal models, hair cell isolation and RT-PCR, injectoporation, whole-mount
414 immunostaining, ABR measurement, DPOAE measurement, vestibular function
415 examination, FM1-43FX uptake experiment, SEM, electrophysiology, noise exposure,
416 yeast two-hybrid, co-IP and western blot, protein purification and co-sedimentation
417 assay, protein labeling and fluorescent imaging, FRAP analysis, and statistical
418 analysis are described in *SI Appendix, SI Materials and Methods*.

419

420 **Data availability.** All study data are included in the article and/or *SI Appendix*.

421

422 **Acknowledgements.** We thank Sen Wang, Xiaomin Zhao, and Haiyan Yu from the
423 core facilities for life and environmental sciences, Shandong University for technical
424 support in SEM and confocal microscopy. This work was supported by grants from
425 National Key Research & Developmental Program of China (2022YFE0131900),
426 National Natural Science Foundation of China (82192861, 82071051), China Ministry
427 of Science and Technology (2021ZD0203304), and Shandong Provincial Natural
428 Science Foundation (ZR2020ZD39).

429

430 **Author contributions.** Z.X. conceived and designed research; N.L., S.L., D.Z., H.D.,
431 Y.X., X.W., and Q.Liu performed research; N.L., S.L., U.M., Q.Lu, W.X., and Z.X.
432 analyzed data; and N.L., U.M., Q.Lu, W.X., and Z.X. wrote the manuscript with
433 contributions from all authors.

434

435 **Competing interests.** The authors declare no competing interests.

436

437

438

439

440

441 **References**

- 442 1. K. Kikuchi, D. Hilding, The development of the organ of Corti in the mouse.
443 *Acta Otolaryngol.* **60**, 207-222 (1965).
- 444 2. A. J. Hudspeth, R. Jacobs, Stereocilia mediate transduction in vertebrate hair
445 cells (auditory system/cilium/vestibular system). *Proc. Natl. Acad. Sci. U.S.A.*
446 **76**, 1506-1509 (1979).
- 447 3. C. Jones *et al.*, Ciliary proteins link basal body polarization to planar cell
448 polarity regulation. *Nat. Genet.* **40**, 69-77 (2008).
- 449 4. J. O. Pickles, S. D. Comis, M. P. Osborne, Cross-links between stereocilia in
450 the guinea pig organ of Corti, and their possible relation to sensory
451 transduction. *Hear. Res.* **15**, 103-112 (1984).
- 452 5. D. N. Furness, C. M. Hackney, Cross-links between stereocilia in the
453 guinea-pig cochlea. *Hear. Res.* **18**, 177-188 (1985).
- 454 6. R. J. Goodyear, W. Marcotti, C. J. Kros, G. P. Richardson, Development and
455 properties of stereociliary link types in hair cells of the mouse cochlea. *J.*
456 *Comp. Neurol.* **485**, 75-85 (2005).
- 457 7. J. A. Assad, G. M. Shepherd, D. P. Corey, Tip-link integrity and mechanical
458 transduction in vertebrate hair cells. *Neuron* **7**, 985-994 (1991).
- 459 8. M. Beurg, R. Fettiplace, J. H. Nam, A. J. Ricci, Localization of inner hair cell
460 mechanotransducer channels using high-speed calcium imaging. *Nat. Neurosci.*
461 **12**, 553-558 (2009).
- 462 9. X. Qiu, U. Müller, Sensing sound: Cellular specializations and molecular force

- 463 sensors. *Neuron* **110**, 3667-3687 (2022).
- 464 10. J. Siemens *et al.*, Cadherin 23 is a component of the tip link in hair-cell
465 stereocilia. *Nature* **428**, 950-955 (2004).
- 466 11. Z. M. Ahmed *et al.*, The tip-link antigen, a protein associated with the
467 transduction complex of sensory hair cells, is protocadherin-15. *J. Neurosci.*
468 **26**, 7022-7034 (2006).
- 469 12. P. Kazmierczak *et al.*, Cadherin 23 and protocadherin 15 interact to form
470 tip-link filaments in sensory hair cells. *Nature* **449**, 87-91 (2007).
- 471 13. A. Lagziel *et al.*, Spatiotemporal pattern and isoforms of cadherin 23 in wild
472 type and waltzer mice during inner ear hair cell development. *Dev. Biol.* **280**,
473 295-306 (2005).
- 474 14. V. Michel *et al.*, Cadherin 23 is a component of the transient lateral links in the
475 developing hair bundles of cochlear sensory cells. *Dev. Biol.* **280**, 281-294
476 (2005).
- 477 15. A. K. Rzadzinska, A. Derr, B. Kachar, K. Noben-Trauth, Sustained cadherin
478 23 expression in young and adult cochlea of normal and hearing-impaired
479 mice. *Hear. Res.* **208**, 114-121 (2005).
- 480 16. R. J. Goodyear, A. Forge, P. K. Legan, G. P. Richardson, Asymmetric
481 distribution of cadherin 23 and protocadherin 15 in the kinocilial links of avian
482 sensory hair cells. *J. Comp. Neurol.* **518**, 4288-4297 (2010).
- 483 17. H. Bolz *et al.*, Mutation of CDH23, encoding a new member of the cadherin
484 gene family, causes Usher syndrome type 1D. *Nat. Genet.* **27**, 108-112 (2001).

- 485 18. J. M. Bork *et al.*, Usher syndrome 1D and nonsyndromic autosomal recessive
486 deafness DFNB12 are caused by allelic mutations of the novel cadherin-like
487 gene CDH23. *Am. J. Hum. Genet.* **68**, 26-37 (2001).
- 488 19. Z. M. Ahmed *et al.*, Mutations of the protocadherin gene PCDH15 cause
489 Usher syndrome type 1F. *Am. J. Hum. Genet.* **69**, 25-34 (2001).
- 490 20. K. N. Alagramam *et al.*, Mutations in the novel protocadherin PCDH15 cause
491 Usher syndrome type 1F. *Hum. Mol. Genet.* **10**, 1709-1718 (2001).
- 492 21. K. N. Alagramam *et al.*, The mouse Ames waltzer hearing-loss mutant is
493 caused by mutation of Pcdh15, a novel protocadherin gene. *Nat. Genet.* **27**,
494 99-102 (2001).
- 495 22. F. Di Palma *et al.*, Mutations in Cdh23, encoding a new type of cadherin,
496 cause stereocilia disorganization in waltzer, the mouse model for Usher
497 syndrome type 1D. *Nat. Genet.* **27**, 103-107 (2001).
- 498 23. M. Schwander *et al.*, A mouse model for nonsyndromic deafness (DFNB12)
499 links hearing loss to defects in tip links of mechanosensory hair cells. *Proc.*
500 *Natl. Acad. Sci. U.S.A.* **106**, 5252-5257 (2009).
- 501 24. B. Kachar, M. Parakkal, M. Kurc, Y. Zhao, P. G. Gillespie, High-resolution
502 structure of hair-cell tip links. *Proc. Natl. Acad. Sci. U.S.A.* **97**, 13336-13341
503 (2000).
- 504 25. N. Grillet *et al.*, Harmonin mutations cause mechanotransduction defects in
505 cochlear hair cells. *Neuron* **62**, 375-387 (2009).
- 506 26. M. Grati, B. Kachar, Myosin VIIa and sans localization at stereocilia upper

507 tip-link density implicates these Usher syndrome proteins in
508 mechanotransduction. *Proc. Natl. Acad. Sci. U.S.A.* **108**, 11476-11481 (2011).

509 27. Y. He, J. Li, M. Zhang, Myosin VII, USH1C, and ANKS4B or USH1G
510 together form condensed molecular assembly via liquid-liquid phase
511 separation. *Cell Rep.* **29**, 974-986 (2019).

512 28. J. Siemens *et al.*, The Usher syndrome proteins cadherin 23 and harmonin
513 form a complex by means of PDZ-domain interactions. *Proc. Natl. Acad. Sci.*
514 *U.S.A.* **99**, 14946-14951 (2002).

515 29. Z. Xu, A. W. Peng, K. Oshima, S. Heller, MAGI-1, a candidate stereociliary
516 scaffolding protein, associates with the tip-link component Cadherin 23. *J.*
517 *Neurosci.* **28**, 11269-11276 (2008).

518 30. K. Noben-Trauth, Q. Zheng, K. R. Johnson, Association of cadherin 23 with
519 polygenic inheritance and genetic modification of sensorineural hearing loss.
520 *Nat. Genet.* **35**, 21-23 (2003).

521 31. J. O. Pickles, G. W. Rouse, M. von Perger, Morphological correlates of
522 mechanotransduction in acousticolateral hair cells. *Scanning Microsc.* **5**,
523 1115-1128 (1991).

524 32. J. O. Pickles, M. P. Osborne, S. D. Comis, Vulnerability of tip links between
525 stereocilia to acoustic trauma in the guinea-pig. *Hear. Res.* **25**, 173-183 (1987).

526 33. M. Takumida, L. Fredelius, D. Bagger-Sjoberg, Y. Harada, J. Wersall, Effect
527 of acoustic overstimulation on the glycocalyx and the ciliary interconnections
528 in the organ of Corti: high resolution scanning electron microscopic

- 529 investigation. *J. Laryngol. Otol.* **103**, 1125-1129 (1989).
- 530 34. L. Wu, L. Pan, C. Zhang, M. Zhang, Large protein assemblies formed by
531 multivalent interactions between cadherin23 and harmonin suggest a stable
532 anchorage structure at the tip link of stereocilia. *J. Biol. Chem.* **287**,
533 33460-33471 (2012).
- 534 35. B. Boeda *et al.*, Myosin VIIa, harmonin and cadherin 23, three Usher I gene
535 products that cooperate to shape the sensory hair cell bundle. *EMBO J.* **21**,
536 6689-6699 (2002).
- 537 36. L. Pan, J. Yan, L. Wu, M. Zhang, Assembling stable hair cell tip link complex
538 via multidentate interactions between harmonin and cadherin 23. *Proc. Natl.*
539 *Acad. Sci. U.S.A.* **106**, 5575-5580 (2009).
- 540 37. A. Bahloul *et al.*, Cadherin-23, myosin VIIa and harmonin, encoded by Usher
541 syndrome type I genes, form a ternary complex and interact with membrane
542 phospholipids. *Hum. Mol. Genet.* **19**, 3557-3565 (2010).
- 543 38. N. Li, H. Du, R. Ren, Y. Wang, Z. Xu, Alternative splicing of Cdh23 exon 68
544 is regulated by RBM24, RBM38, and PTBP1. *Neural Plast.* **2020**, 8898811
545 (2020).
- 546 39. Y. Wang *et al.*, RBM24 is required for mouse hair cell development through
547 regulating pre-mRNA alternative splicing and mRNA stability. *J. Cell. Physiol.*
548 **238**, 1095-1110 (2023).
- 549 40. J. M. Husbands, S. A. Steinberg, R. Kurian, J. C. Saunders, Tip-link integrity
550 on chick tall hair cell stereocilia following intense sound exposure. *Hear. Res.*

- 551 **135**, 135-145 (1999).
- 552 41. Y. Zhao, E. N. Yamoah, P. G. Gillespie, Regeneration of broken tip links and
553 restoration of mechanical transduction in hair cells. *Proc. Natl. Acad. Sci.*
554 *U.S.A.* **93**, 15469-15474 (1996).
- 555 42. A. A. Indzhukulian *et al.*, Molecular remodeling of tip links underlies
556 mechanosensory regeneration in auditory hair cells. *PLoS Biol.* **11**, e1001583
557 (2013).
- 558 43. R. G. Alonso, M. Tobin, P. Martin, A. J. Hudspeth, Fast recovery of disrupted
559 tip links induced by mechanical displacement of hair bundles. *Proc. Natl.*
560 *Acad. Sci. U.S.A.* **117**, 30722-30727 (2020).
- 561 44. J. Mianne *et al.*, Correction of the auditory phenotype in C57BL/6N mice via
562 CRISPR/Cas9-mediated homology directed repair. *Genome Med.* **8**, 16 (2016).
- 563 45. J. Jeng *et al.*, Pathophysiological changes in inner hair cell ribbon synapses in
564 the ageing mammalian cochlea. *J. Physiol.* **598**, 4339-4355 (2020).
- 565 46. H. Nie *et al.*, Plasma membrane targeting of Protocadherin 15 is regulated by
566 the Golgi-associated chaperone protein PIST. *Neural Plast.* **2016**, 8580675
567 (2016).
- 568 47. A. Ballesteros, M. Yadav, R. Cui, K. Kurima, B. Kachar, Selective binding and
569 transport of protocadherin 15 isoforms by stereocilia unconventional myosins
570 in a heterologous expression system. *Sci. Rep.* **12**, 13764 (2022).
- 571 48. Z. Xu, K. Oshima, S. Heller, PIST regulates the intracellular trafficking and
572 plasma membrane expression of cadherin 23. *BMC Cell Biol.* **11**, 80 (2010).

573 49. M. Sotomayor, W. A. Weihofen, R. Gaudet, D. P. Corey, Structure of a
574 force-conveying cadherin bond essential for inner-ear mechanotransduction.
575 *Nature* **492**, 128-132 (2012).
576
577
578
579
580
581
582
583
584
585
586
587
588
589
590
591
592
593
594

595 **Figure Legends**

596 **Fig. 1.** CDH23 isoforms show different expression patterns in mouse cochlea. (A)
597 Schematic drawing of hair cell stereocilia and tip links. (B) Schematic drawing of
598 various CDH23 isoforms. (C) RT-PCR results showing expression of *Cdh23(+68)* and
599 *Cdh23(-68)* transcripts in mouse cochlear sensory epithelium and spiral ganglion cells
600 at different ages as indicated. *β-actin* was included as an internal control. (D) RT-PCR
601 results showing expression of *Cdh23(+68)* and *Cdh23(-68)* transcripts in mouse
602 cochlea and isolated cochlear hair cells at P0 and P15. *Sox2* was included as an
603 internal control for supporting cells. (E) Injectoporation results showing the
604 subcellular localization of CDH23 V1, V2, and V3 isoforms in cochlear hair cells.
605 Shown are single confocal images taken from the middle cochlear turn. HA-tagged
606 CDH23 isoforms were recognized with anti-HA antibody (green). Hair cells were
607 labelled using an anti-MYO7A antibody (red). Stereocilia were visualized using
608 TRITC-conjugated phalloidin (magenta). Scale bar, 10 μm.

609

610 **Fig. 2.** *Cdh23^{Δ68/Δ68}* mice show hearing loss but no balance deficits. (A) Schematic
611 drawing of the strategy for construction of *Cdh23* exon 68 knockout mice. Exons are
612 indicated by numbered boxes. Deleted region is labelled in red. The positions of
613 gRNA targets are indicated by arrows. (B) RT-PCR results showing expression of
614 *Cdh23(+68)* and *Cdh23(-68)* transcripts in the cochlea from P5 wild-type (WT),
615 *Cdh23^{+/-Δ68}*, *Cdh23^{Δ68/Δ68}*, and *Cdh23^{v2J/v2J}* mice. *β-actin* was included as an internal
616 control. (C) ABR thresholds to click stimuli in *Cdh23^{+/-Δ68}* and *Cdh23^{Δ68/Δ68}* mice of

617 different ages as indicated. (D) ABR thresholds to pure tone stimuli in P18
618 *Cdh23*^{+/ Δ 68} and *Cdh23* ^{Δ 68/ Δ 68} mice. (E) DPOAE thresholds to pure tone stimuli in P30
619 *Cdh23*^{+/ Δ 68} and *Cdh23* ^{Δ 68/ Δ 68} mice. (F) - (K) Vestibular function of 7-month-old
620 *Cdh23*^{+/ Δ 68} and *Cdh23* ^{Δ 68/ Δ 68} mice was evaluated by performing rotarod test (F),
621 swimming test (G), tail hanging reflex (H), stereotyped circling movement (I),
622 retropulsion (J), and head bobbing (K). *Cdh23*^{v2J/v2J} mice were included as positive
623 control. The number of animals for each group is indicated in the brackets or by the
624 number of symbols. The statistic test was performed via two-way ANOVA with
625 Šídák's multiple comparisons test (for panels C - E), two-way ANOVA with Dunnett's
626 multiple comparisons test (for panel F), or Kruskal-Wallis test with Dunn's multiple
627 comparisons (for panels G - K). ns, not significant; *, p<0.05; **, p<0.01; ***,
628 p<0.001; ****, p<0.0001.

629

630 **Fig. 3.** Tip-link formation and FM1-43FX uptake are unaffected in young
631 *Cdh23* ^{Δ 68/ Δ 68} mice. (A) Localization of CDH23 in the stereocilia of P8 *Cdh23*^{+/ Δ 68}
632 and *Cdh23* ^{Δ 68/ Δ 68} OHCs and IHCs was examined by performing whole-mount
633 immunostaining using an antibody against the cytoplasmic tail of CDH23 (green).
634 Stereociliary F-actin was visualized with TRITC-conjugated phalloidin (magenta).
635 *Cdh23*^{v2J/v2J} mice were included as negative control. Shown are single confocal
636 images taken from the middle cochlear turn. (B) Quantification of CDH23
637 immunoreactivity in middle-turn hair bundles according to the whole-mount
638 immunostaining results similar to (A). (C) The morphology of hair bundles from P8

639 *Cdh23*^{+/ Δ 68} and *Cdh23* ^{Δ 68/ Δ 68} OHCs and IHCs was examined by SEM. *Cdh23*^{v2J/v2J}
640 mice were included as negative control. Shown are single images taken from the
641 middle cochlear turn. (D) Percentage of second-row stereocilia with beveled tips in
642 middle-turn OHCs and IHCs was calculated from the SEM results similar to (C). (E)
643 Tip links of P8 *Cdh23*^{+/ Δ 68} and *Cdh23* ^{Δ 68/ Δ 68} OHCs and IHCs were examined by
644 SEM. *Cdh23*^{v2J/v2J} mice were included as negative control. Shown are single images
645 taken from the middle cochlear turn. Triangles indicate stereocilia with tip links;
646 asterisks indicate stereocilia without tip links. (F) Percentage of second- and third-row
647 stereocilia with tip links in middle-turn OHCs and IHCs was calculated from the SEM
648 results similar to (E). (G) FM1-43FX uptake by *Cdh23*^{+/ Δ 68} and *Cdh23* ^{Δ 68/ Δ 68}
649 cochlear hair cells at different ages as indicated was examined using confocal
650 microscope. Shown are single confocal images taken from the middle cochlear turn.
651 (H) FM1-43FX uptake in middle-turn cochlear hair cells was quantified according to
652 the results similar to (G). Scale bars, 5 μ m in (A), 1 μ m in (C) and (E), 200 nm in the
653 insets of (E), and 10 μ m in (G). The cell numbers for each group are indicated by the
654 numbers of symbols (or 50 for panel H) from at least three animals. The statistic test
655 was performed via one-way ANOVA with Dunnett's multiple comparisons test (for
656 panel B, F, and OHCs in panel D), Kruskal-Wallis test with Dunn's multiple
657 comparisons (for IHCs in panel D), or Two-way ANOVA with Šídák's multiple
658 comparisons test (for panel H). ns, not significant; ****, p<0.0001.

659

660 **Fig. 4.** MET currents are unaffected in young *Cdh23* ^{Δ 68/ Δ 68} mice. (A) Representative

661 MET currents induced by fluid jet were examined in OHCs from *Cdh23*^{+/ Δ 68} and
662 *Cdh23* ^{Δ 68/ Δ 68} mice. A 40-Hz sinusoidal fluid jet was delivered to the hair bundle. (B)
663 Averaged peak MET currents from similar data as shown in (A). (C) Representative
664 MET currents induced by a stiff probe were examined in OHCs from *Cdh23*^{+/ Δ 68} and
665 *Cdh23* ^{Δ 68/ Δ 68} mice. A set of 10 msec-hair bundle deflections were delivered ranging
666 from -300 nm to 1000 nm at 100 nm steps. (D) Activation time constant ($\tau_{\text{activation}}$) in
667 *Cdh23*^{+/ Δ 68} OHCs (0.1261 msec) and *Cdh23* ^{Δ 68/ Δ 68} OHCs (0.1308 msec). (E) Time
668 constants of fast adaptation (τ_{fast}) in *Cdh23*^{+/ Δ 68} OHCs (0.7614 msec) and
669 *Cdh23* ^{Δ 68/ Δ 68} OHCs (0.7868 msec). (F) Time constants of slow adaptation (τ_{slow}) in
670 *Cdh23*^{+/ Δ 68} OHCs (9.101 msec) and *Cdh23* ^{Δ 68/ Δ 68} OHCs (13.22 msec). (G)
671 Voltage-gated currents were recorded from *Cdh23*^{+/ Δ 68} and *Cdh23* ^{Δ 68/ Δ 68} OHCs. The
672 membrane potential was altered from -150 mV to +110 mV at 20 mV steps. (H) I-V
673 curves were drawn from data similar to panel (G). In all panels, data were collected
674 from P6-P8 OHCs from at least three mice with *Cdh23*^{+/ Δ 68} shown in black and
675 *Cdh23* ^{Δ 68/ Δ 68} shown in red. Cell number is indicated in the brackets. The statistic test
676 was performed via student's two-tailed unpaired *t* test. ns, not significant.

677

678 **Fig. 5.** Stereocilia maintenance is affected in adult *Cdh23* ^{Δ 68/ Δ 68} cochlear hair cells.
679 (A) Hair bundle morphology from *Cdh23*^{+/ Δ 68} and *Cdh23* ^{Δ 68/ Δ 68} mice at different
680 ages and cochlear positions as indicated was examined by SEM. (B) OHC hair bundle
681 numbers along successive 20-IHC intervals was calculated according to the SEM
682 results similar to (A). (C) High-magnification SEM images of middle-turn OHC hair

683 bundles from *Cdh23*^{+/ Δ 68} and *Cdh23* ^{Δ 68/ Δ 68} mice at different ages as indicated.
684 First-row stereocilia are indicated in red; second-row stereocilia are indicated in
685 yellow; third-row stereocilia are indicated in blue. (D) Numbers of third-row
686 stereocilia with normal height per OHC at middle cochlear turn was calculated
687 according to the SEM results similar to (C). Scale bars, 20 μ m in (A), 1 μ m in (C).
688 The sample numbers for each group are indicated by the numbers of symbols from at
689 least three animals. The statistic test was performed via two-way ANOVA with
690 Tukey's multiple comparisons test. ns, not significant; *, p<0.05; ***, p<0.001; ****,
691 p<0.0001.

692

693 **Fig. 6.** Tip links and FM1-43FX uptake are affected in adult *Cdh23* ^{Δ 68/ Δ 68} mice. (A)
694 High-magnification SEM images of middle-turn IHC hair bundles from *Cdh23*^{+/ Δ 68}
695 and *Cdh23* ^{Δ 68/ Δ 68} mice at different ages as indicated. First-row stereocilia are
696 indicated in red; second-row stereocilia are indicated in yellow; third-row stereocilia
697 are indicated in blue. (B) Numbers of third-row stereocilia with normal height per
698 IHC at middle cochlear turn was calculated according to the SEM results similar to
699 (A). (C) Percentage of second-row stereocilia with beveled tips in middle-turn IHCs
700 was calculated from the SEM results similar to (A). (D) Tip links of 8-month-old
701 *Cdh23*^{+/ Δ 68} and *Cdh23* ^{Δ 68/ Δ 68} OHCs and IHCs were examined by SEM. Shown are
702 single images taken from the middle cochlear turn. Triangles indicate stereocilia with
703 tip links; asterisks indicate stereocilia without tip links. (E) Percentage of second- and
704 third-row stereocilia with tip links in middle-turn OHCs and IHCs was calculated

705 from the SEM results similar to (D). (F) Localization of CDH23 in the stereocilia of
706 5-month-old *Cdh23*^{+/ Δ 68} and *Cdh23* ^{Δ 68/ Δ 68} mice was examined by performing
707 whole-mount immunostaining using an antibody against the cytoplasmic tail of
708 CDH23 (green). Stereociliary F-actin was visualized with TRITC-conjugated
709 phalloidin (magenta). Shown are single confocal images taken from the middle
710 cochlear turn. (G) Quantification of CDH23 immunoreactivity in middle-turn cochlear
711 hair cells according to the whole-mount immunostaining results similar to (F). (H)
712 FM1-43FX uptake by 5-month-old *Cdh23*^{+/ Δ 68} and *Cdh23* ^{Δ 68/ Δ 68} cochlear hair cells
713 was examined using confocal microscope. Shown are single images taken from the
714 middle cochlear turn. (I) FM1-43FX uptake in middle-turn cochlear hair cells was
715 quantified according to the results similar to (H). Scale bars, 1 μ m in (A) and (D), 200
716 nm in the insets of (D), 5 μ m in (F), and 10 μ m in (H). The cell numbers for each
717 group are indicated by the numbers of symbols from at least three animals. The
718 statistic test was performed via two-way ANOVA with Tukey's multiple comparisons
719 test (for panels B and C), Mann-Whitney test (for panel E), or student's *t* test (for
720 panels G and I). ns, not significant; **, $p < 0.01$; ****, $p < 0.0001$.

721

722 **Fig. 7.** *Cdh23* ^{Δ 68/ Δ 68} mice show increased acoustic vulnerability. (A - B)
723 One-month-old *Cdh23*^{+/ Δ 68} and *Cdh23* ^{Δ 68/ Δ 68} mice were exposed to a broadband
724 noise of 2-20 kHz at 96 dB SPL for 2 h, and mice of the same genotypes and ages
725 without noise exposure were included as control groups (Ctl). Hearing thresholds to
726 pure tone or click stimuli 1 day (A) or 14 days (B) after noise treatment were analyzed

727 by performing ABR measurements. (C) Hair bundle morphology from *Cdh23*<sup>+/ Δ ⁶⁸
728 and *Cdh23* <sup>Δ ⁶⁸/ Δ ⁶⁸ basal-turn hair cells at different time after noise exposure was
729 examined by SEM. (D) OHC hair bundle numbers along successive 20-IHC intervals
730 in the basal cochlear turn was calculated according to the SEM results similar to (C).
731 (E) High-magnification SEM images of middle-turn OHC hair bundles from
732 *Cdh23*<sup>+/ Δ ⁶⁸ and *Cdh23* <sup>Δ ⁶⁸/ Δ ⁶⁸ mice at different time after noise exposure. First-row
733 stereocilia are indicated in red; second-row stereocilia are indicated in yellow;
734 third-row stereocilia are indicated in blue. (F) Numbers of third-row stereocilia with
735 normal height per OHC in the middle cochlear turn was calculated according to the
736 SEM results similar to (E). Scale bars, 20 μ m in (C), 1 μ m in (E). The sample
737 numbers for each group are indicated by the numbers of symbols from at least three
738 animals. The statistic test was performed via two-way ANOVA with Tukey's multiple
739 comparisons test (for panel D, F and click measurements in panels A, B), or two-way
740 ANOVA with Šídák's multiple comparisons test (for pure-tone measurements in
741 panels A, B). ns, not significant; *, p<0.05; **, p<0.01; ***, p<0.001; ****,
742 p<0.0001.</sup></sup></sup></sup>

743

744 **Fig. 8.** Stereocilia maintenance and FM1-43FX uptake are affected in noise-exposed
745 *Cdh23* <sup>Δ ⁶⁸/ Δ ⁶⁸ mice. (A) High-magnification SEM images of middle-turn IHC hair
746 bundles from *Cdh23*<sup>+/ Δ ⁶⁸ and *Cdh23* <sup>Δ ⁶⁸/ Δ ⁶⁸ mice at different time after noise
747 exposure. First-row stereocilia are indicated in red; second-row stereocilia are
748 indicated in yellow; third-row stereocilia are indicated in blue. (B) Numbers of</sup></sup></sup>

749 third-row stereocilia with normal height per IHC in the middle cochlear turn was
750 calculated according to the SEM results similar to (A). (C) Percentage of second-row
751 stereocilia with beveled tips in middle-turn hair cells was calculated from the SEM
752 results similar to (A). (D) Tip links of *Cdh23*<sup>+/ Δ ⁶⁸ and *Cdh23* <sup>Δ ⁶⁸/ Δ ⁶⁸ OHCs and IHCs
753 at 14 days after noise exposure were examined by SEM. Shown are single images
754 taken from the middle cochlear turn. Triangles indicate stereocilia with tip links. (E)
755 Percentage of second- and third-row stereocilia with tip links in middle-turn hair cells
756 was calculated from the SEM results similar to (D). (F) Localization of CDH23 in the
757 stereocilia of *Cdh23*<sup>+/ Δ ⁶⁸ and *Cdh23* <sup>Δ ⁶⁸/ Δ ⁶⁸ mice at different time after noise exposure
758 was examined by performing whole-mount immunostaining using an antibody against
759 the cytoplasmic tail of CDH23 (green). Stereociliary F-actin was visualized with
760 TRITC-conjugated phalloidin (magenta). Shown are single confocal images taken
761 from the middle cochlear turn. (G) Quantification of CDH23 immunoreactivity in
762 middle-turn hair bundles according to the whole-mount immunostaining results
763 similar to (F). (H) FM1-43FX uptake by *Cdh23*<sup>+/ Δ ⁶⁸ and *Cdh23* <sup>Δ ⁶⁸/ Δ ⁶⁸ cochlear hair
764 cells at different time after noise exposure was examined using confocal microscope.
765 Shown are single images taken from the middle cochlear turn. (I) FM1-43FX uptake
766 in middle-turn hair cells was quantified according to the results similar to (H). Scale
767 bars, 1 μ m in (A) and (D), 200 nm in the insets of (D), 2.5 μ m in (F), and 10 μ m in
768 (H). The cell numbers for each group are indicated by the numbers of symbols from at
769 least three animals. The statistic test was performed via two-way ANOVA with
770 Tukey's multiple comparisons test (for panels B, G and I), Mann-Whitney test (for</sup></sup></sup></sup></sup></sup>

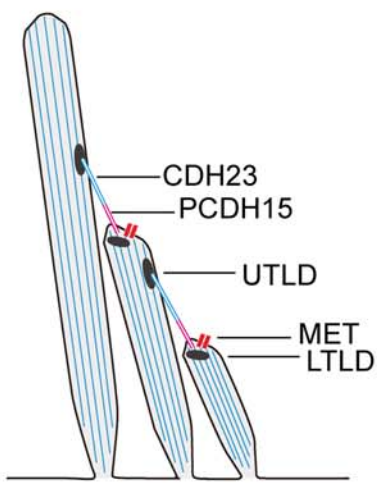
771 panel C), or Mann-Whitney test (for panel E). ns, not significant; ***, $p < 0.001$; ****, $p < 0.0001$.

773

774 **Fig. 9.** Exon 68 is important for CDH23 dimerization and condensate formation. (A)
775 Interaction between CDH23 isoforms examined by performing yeast two-hybrid assay.
776 Left: Transformation efficiency is examined on SD-Leu-Trp medium, and
777 protein-protein interaction is examined on SD-Leu-Trp-His-Ade medium. Right:
778 Quantification of protein-protein interaction according to results similar to left. Nubl
779 and pPR3-N are included as positive and negative controls, respectively. (B)
780 Interaction between CDH23 isoforms examined by co-IP. Expression vectors were
781 transfected into HEK293T cells to express GFP- or MYC-tagged CDH23 isoforms,
782 and cell lysates were subjected to immunoprecipitation. IP indicates antibody used for
783 immunoprecipitation, and WB indicates antibody used for detection. (C)
784 Co-sedimentation results of CDH23 cytoplasmic tail (50 μ M) showing that
785 CDH23(+68) cytoplasmic tail was much more enriched in the pellet than CDH23(-68)
786 cytoplasmic tail. S indicates supernatant, and P indicates pellet. (D) Co-sedimentation
787 results of CDH23(+68) cytoplasmic tail mixed with harmonin NPDZ12 fragment.
788 Both proteins were enriched in the pellet and the pellet fraction of the mixture exceeds
789 that of CDH23(+68) cytoplasmic tail alone. (E) Fluorescence images showing that
790 CDH23(+68) cytoplasmic tail/harmonin NPDZ12 fragment forms larger droplets than
791 CDH23(-68) cytoplasmic tail/harmonin NPDZ12 fragment. CDH23 cytoplasmic tail
792 and harmonin NPDZ12 fragment were labeled with Cy3 and Alexa 488, respectively.

793 Labeled proteins were added at a ratio of 1%. CDH23 cytoplasmic tail: 180 μ M,
794 harmonin NPDZ12 fragment: 45 μ M. (F) Fluorescence images showing that the phase
795 separation capacity of CDH23 cytoplasmic tail/harmonin NPDZ12 fragment is
796 concentration-dependent. The concentration ratio of CDH23 cytoplasmic tail:
797 harmonin NPDZ12 fragment is 4:1, and proteins were labeled in the same way as in
798 (E). (G) Images showing the recovery process of CDH23(+68) cytoplasmic tail
799 fluorescence after photobleaching. Proteins were labeled in the same way as in (E). (H)
800 Quantification of the recovery process of CDH23(+68) cytoplasmic tail fluorescence
801 according to results similar to (G) (n=3). Scale bars, 10 μ m in (E) and (F), 5 μ m in (G).
802 The statistic test was performed via one-way ANOVA with Dunnett's multiple
803 comparisons test (for panel A). ns, not significant; **, p<0.01; ***, p<0.001.

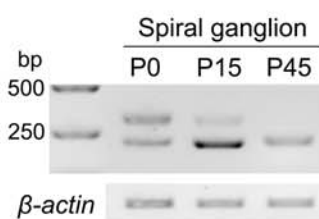
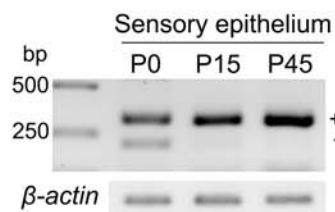
A



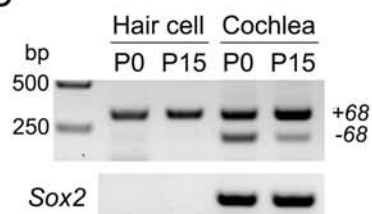
B



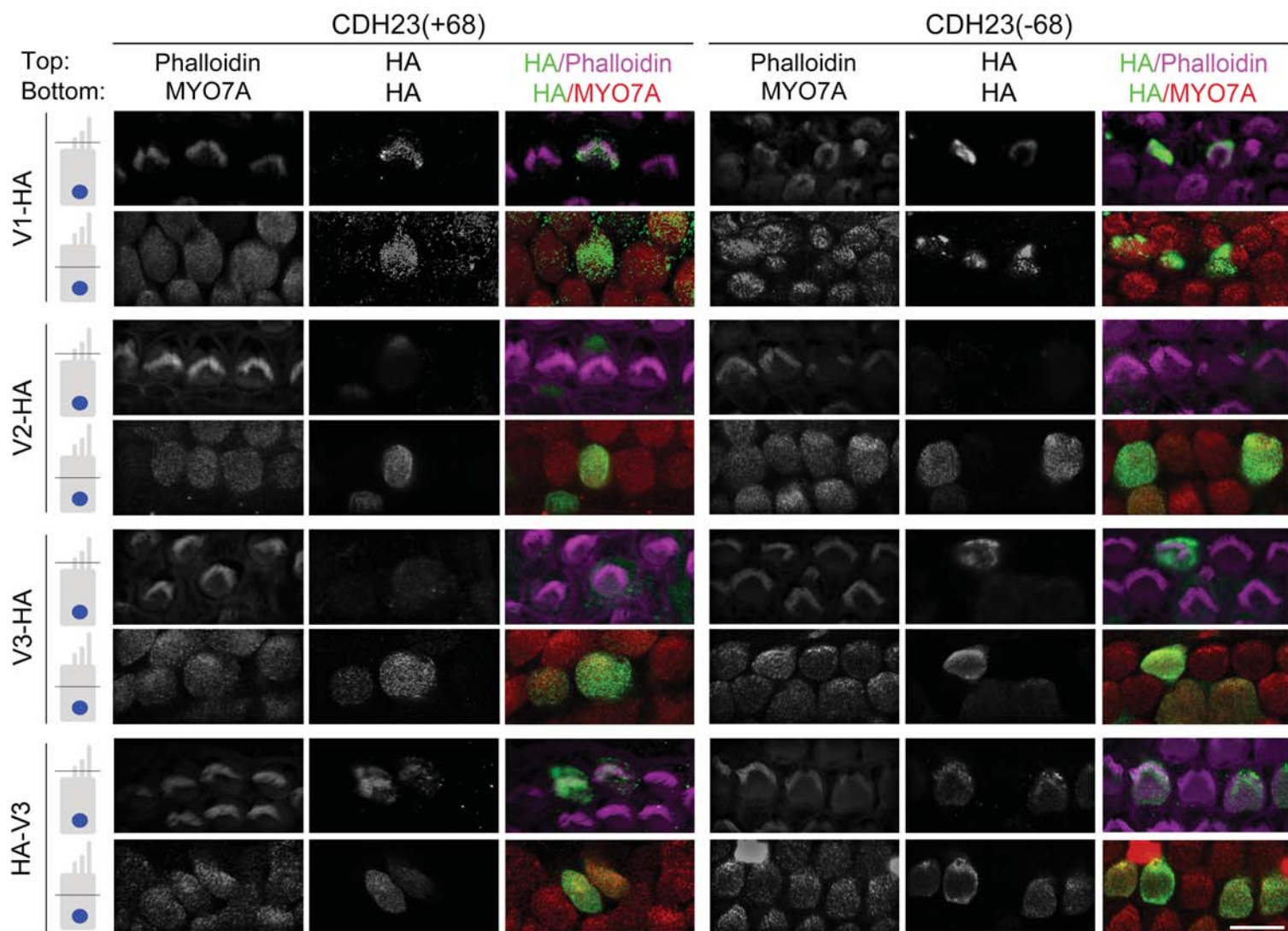
C

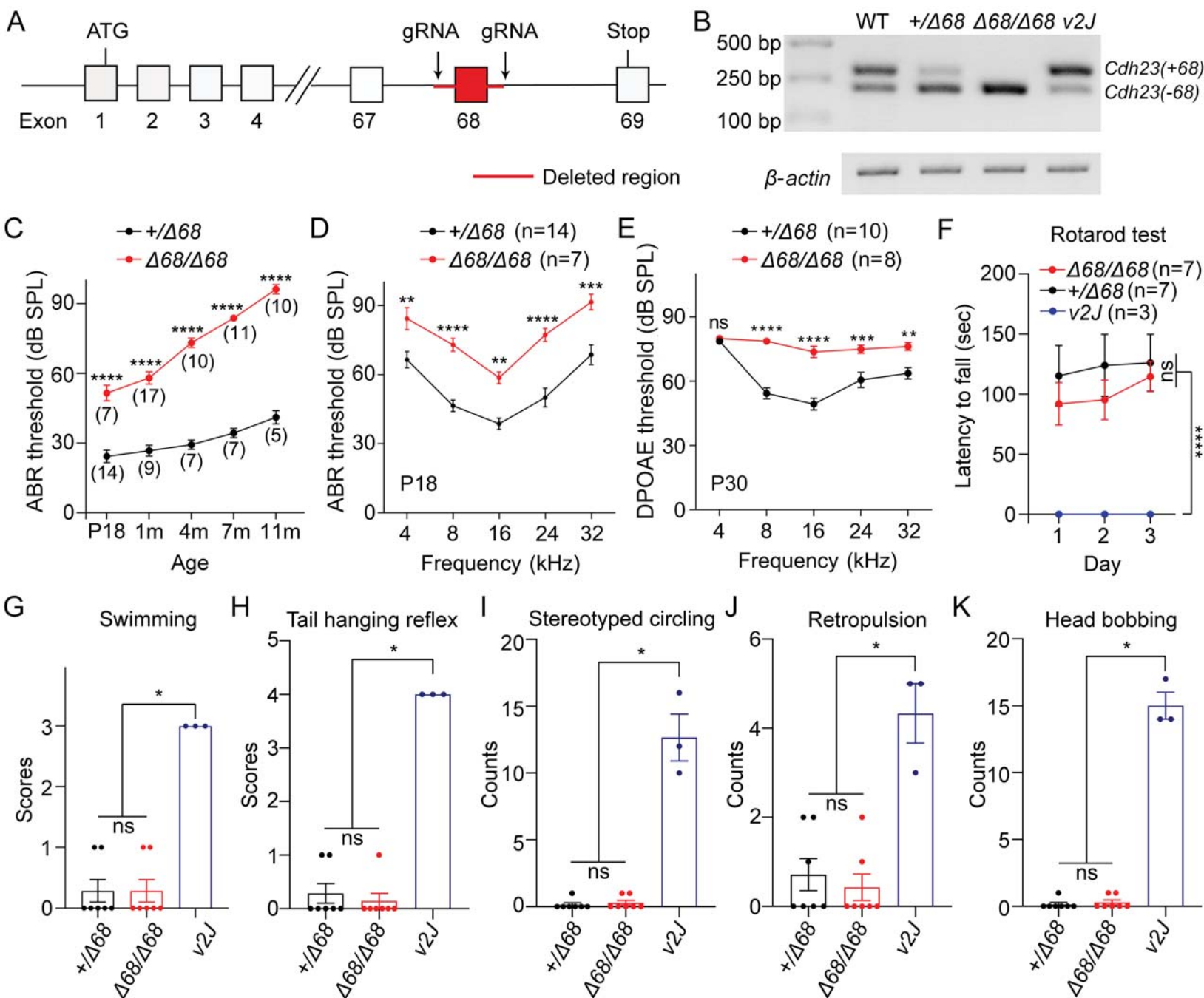


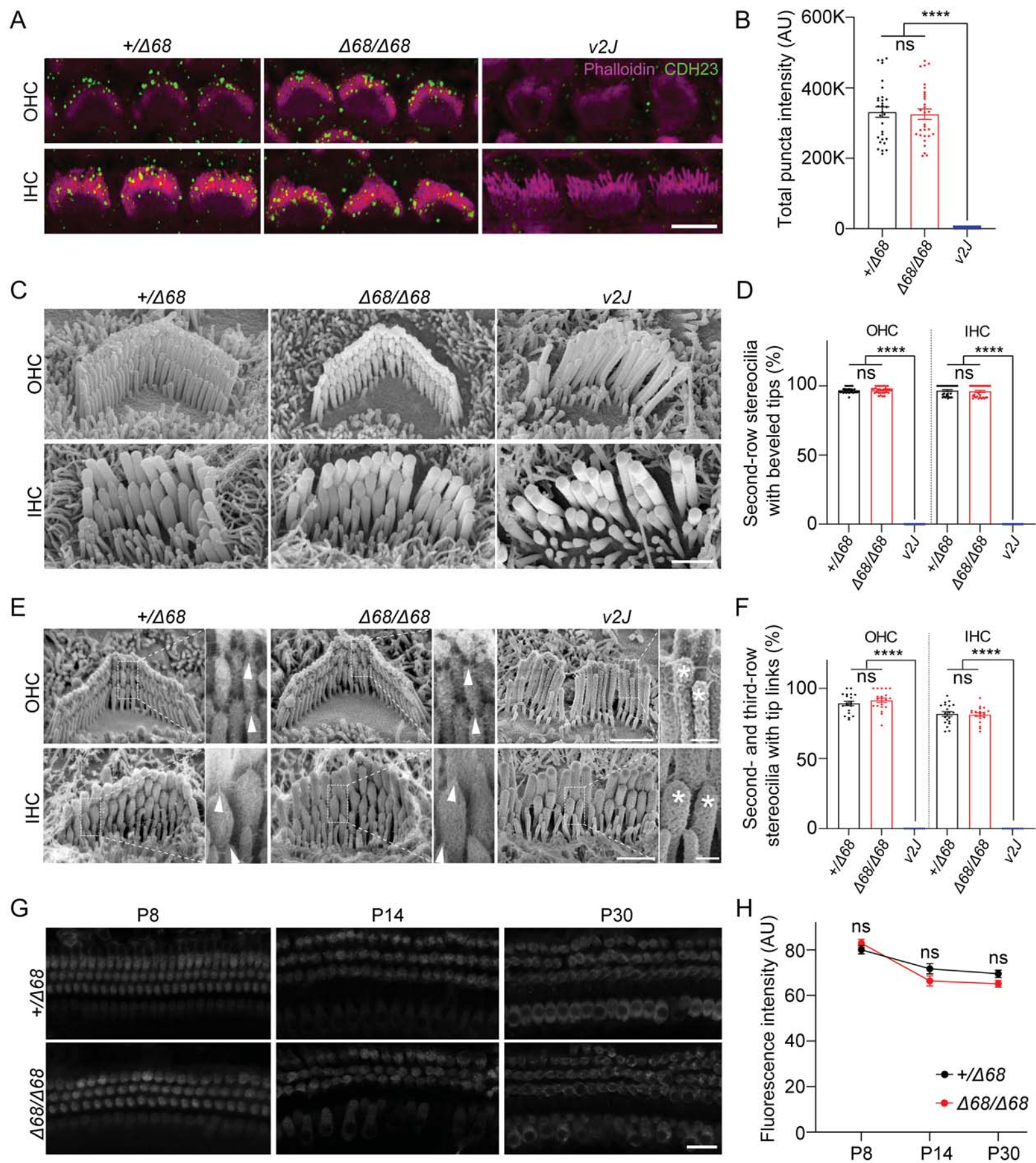
D

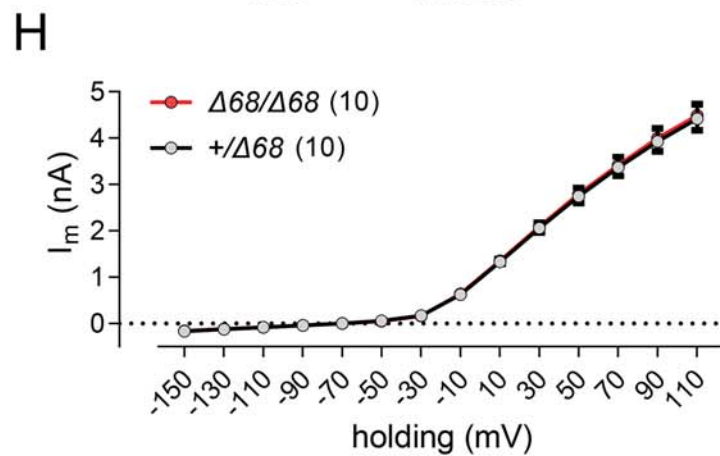
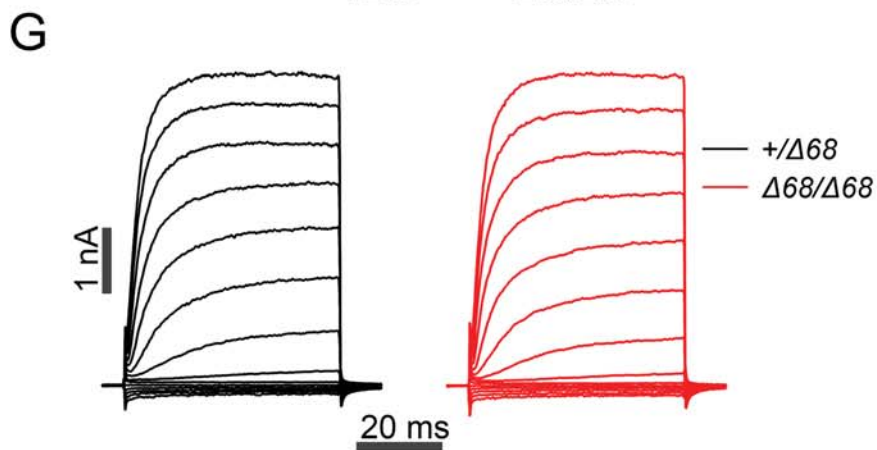
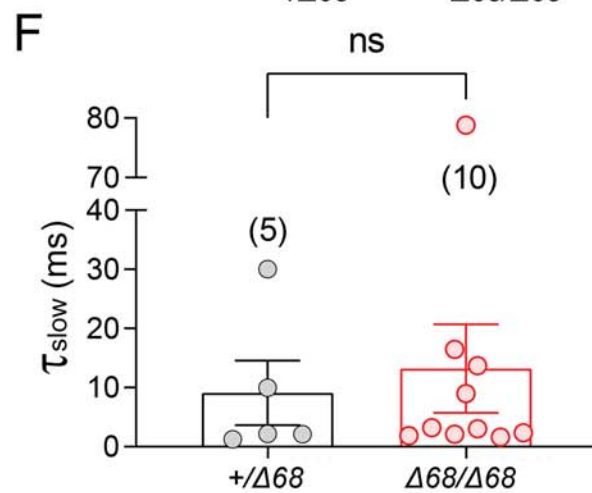
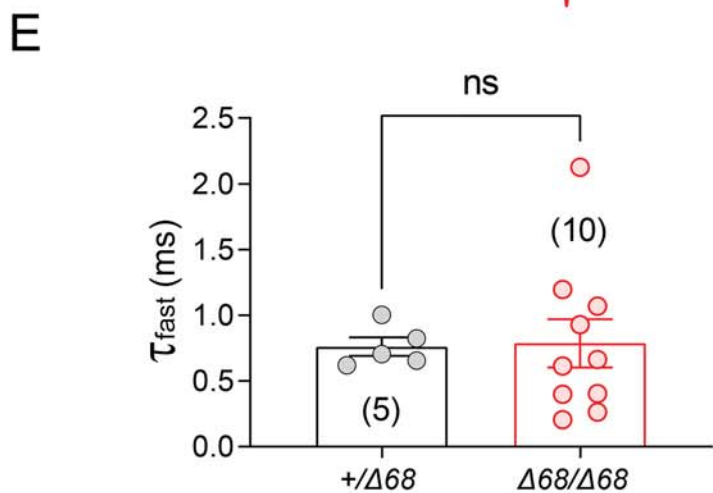
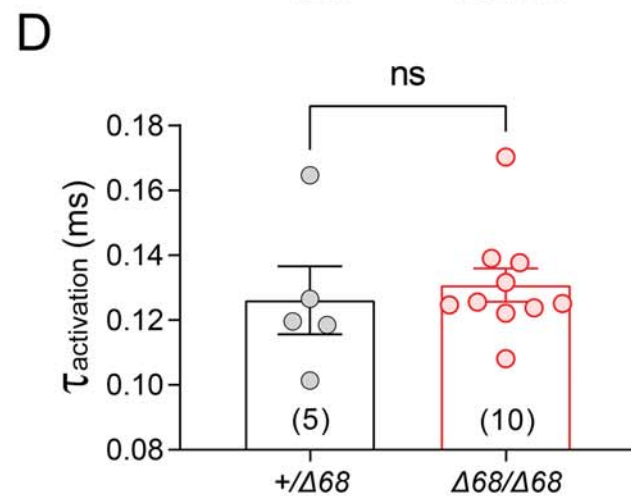
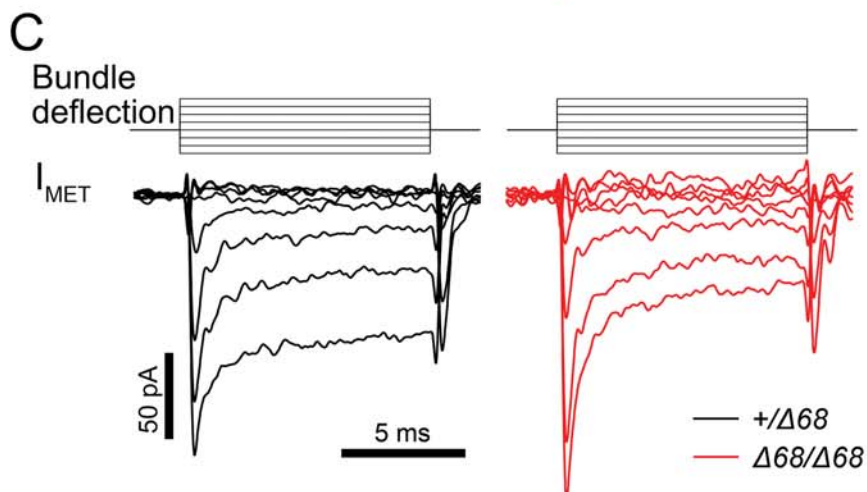
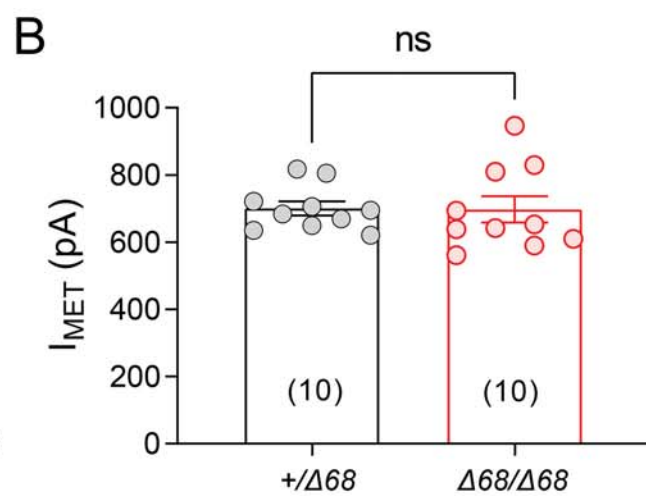
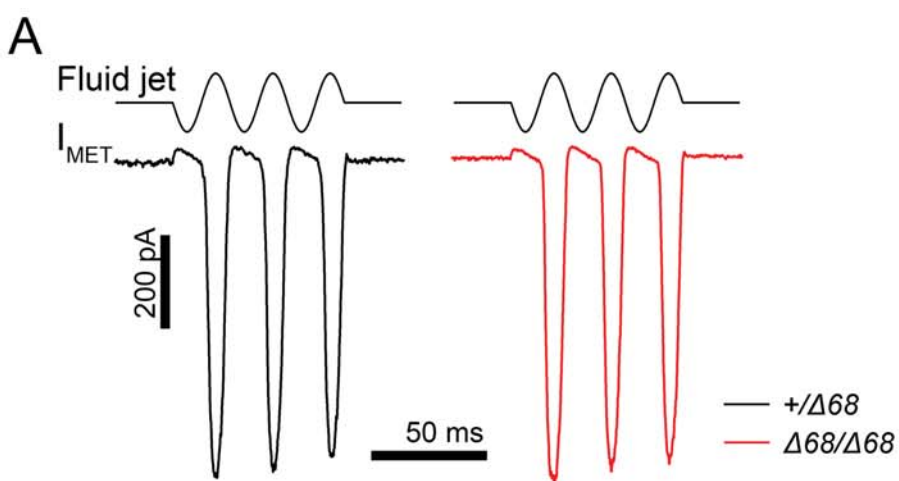


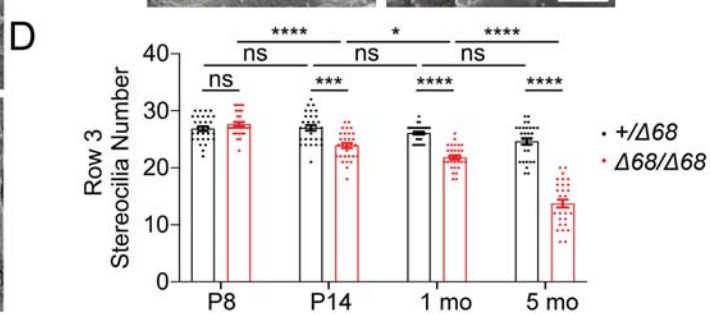
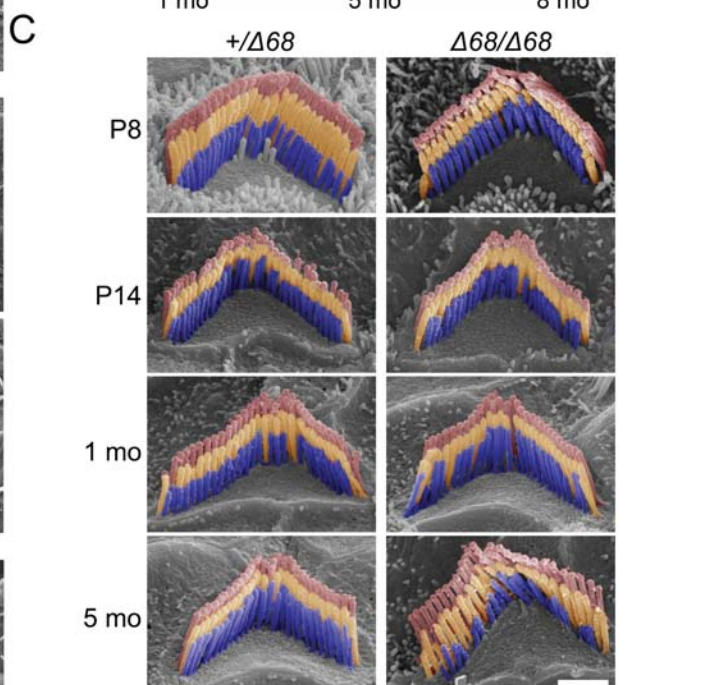
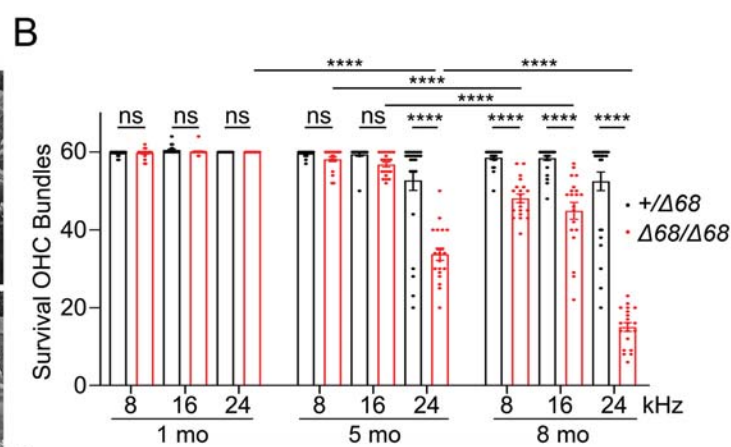
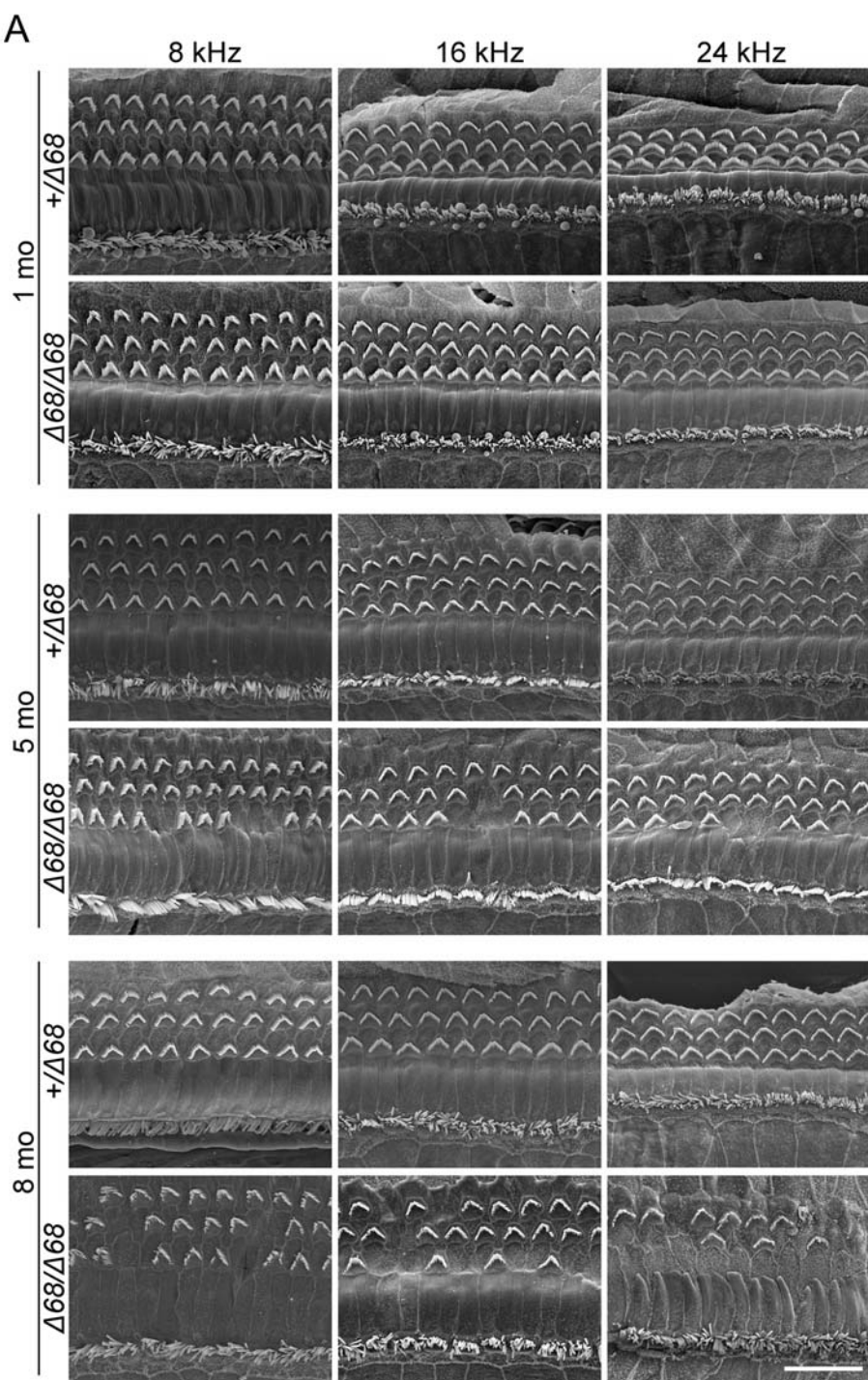
E

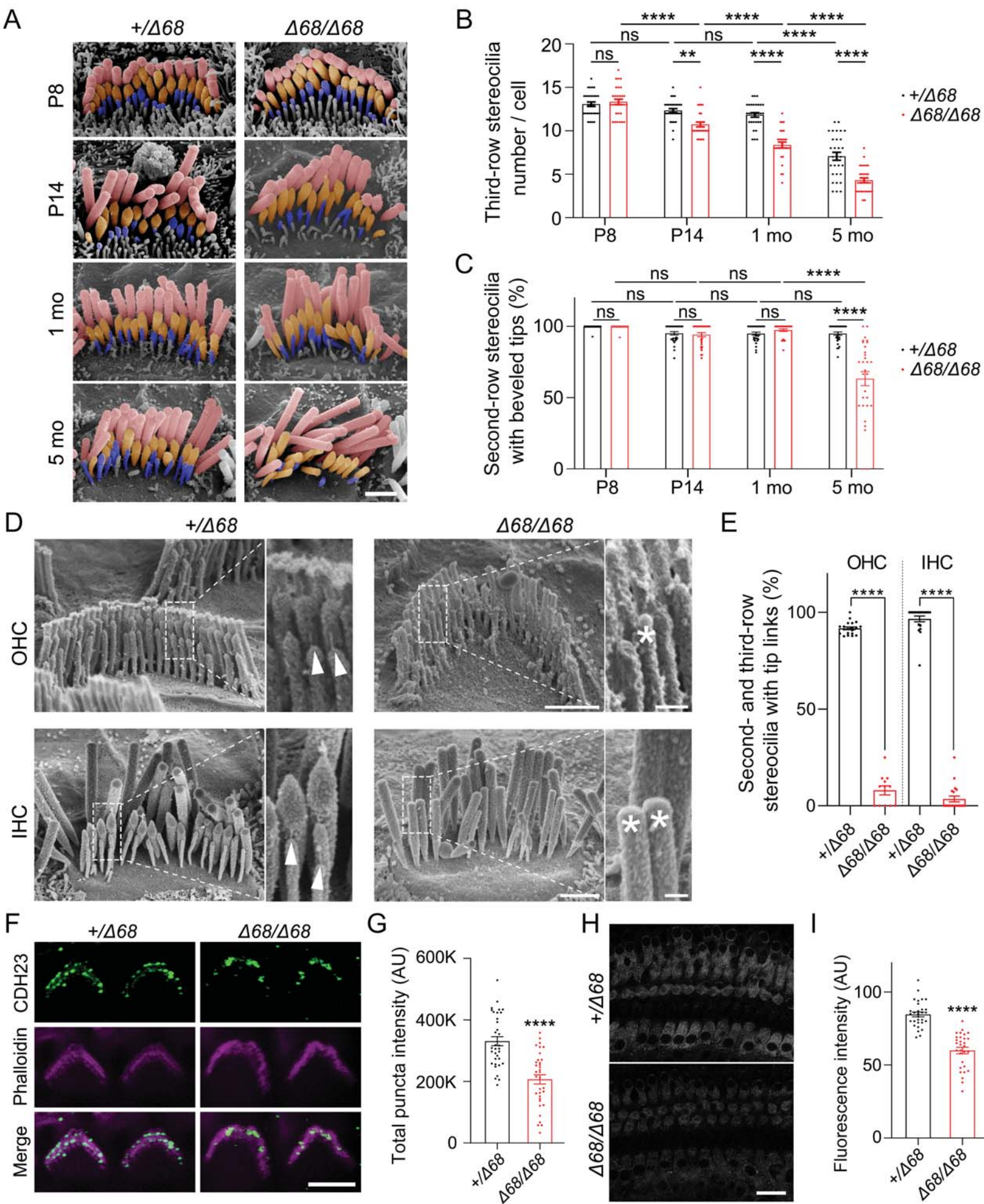


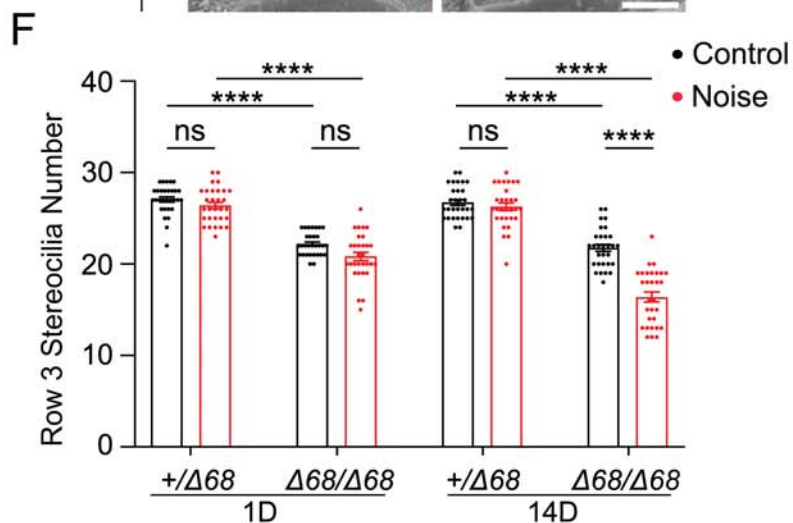
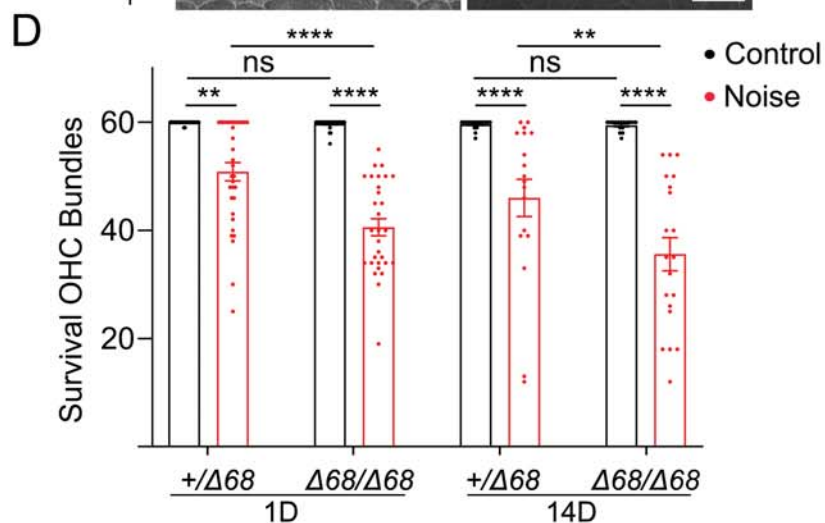
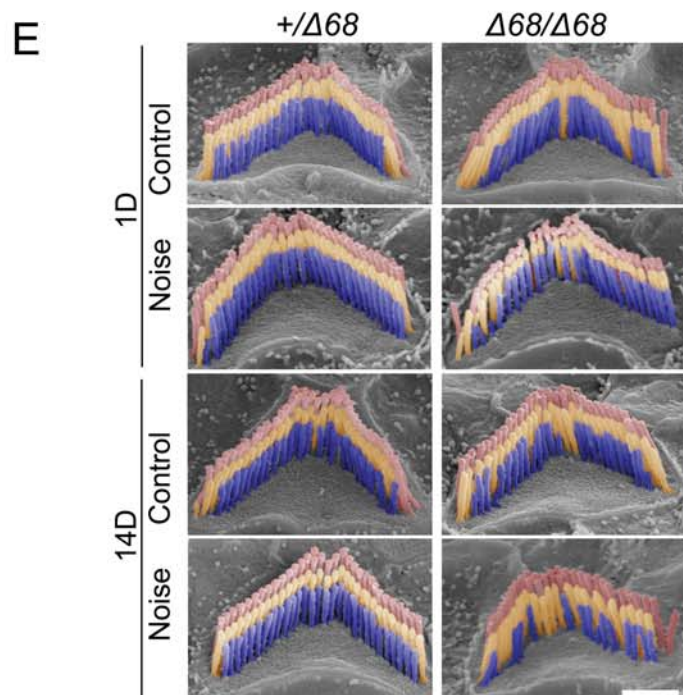
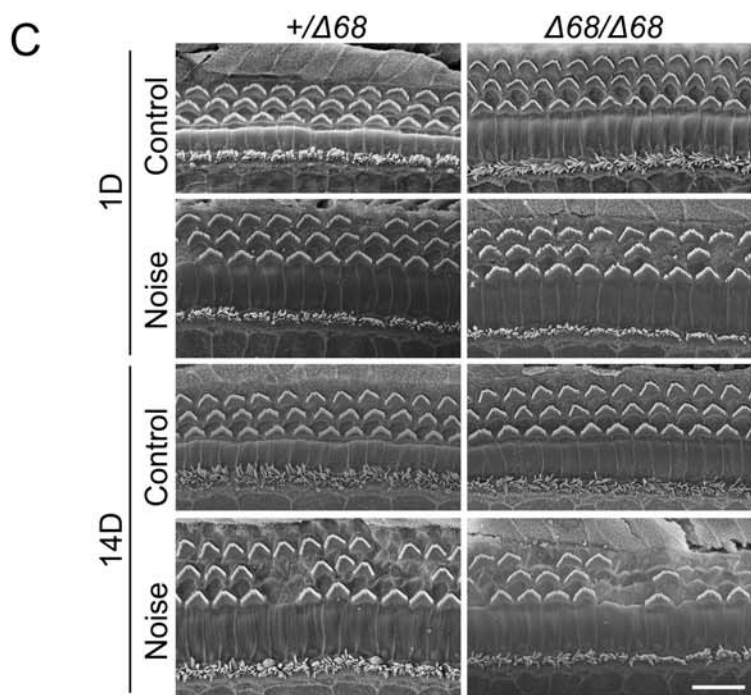
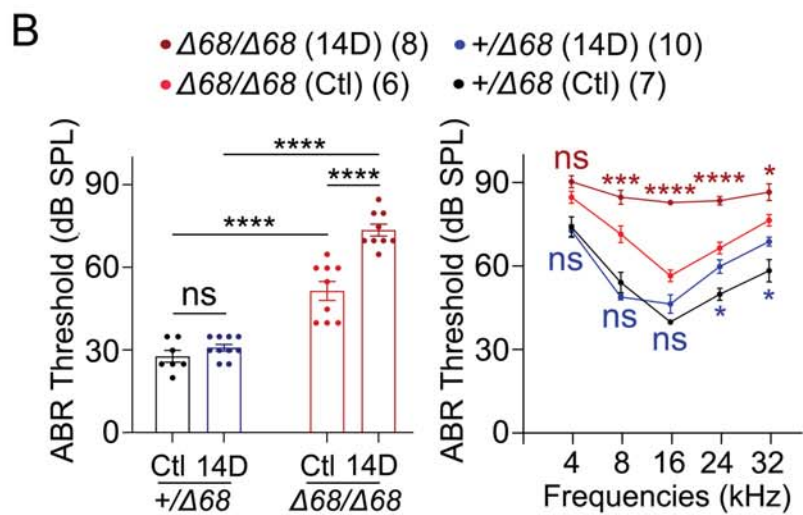
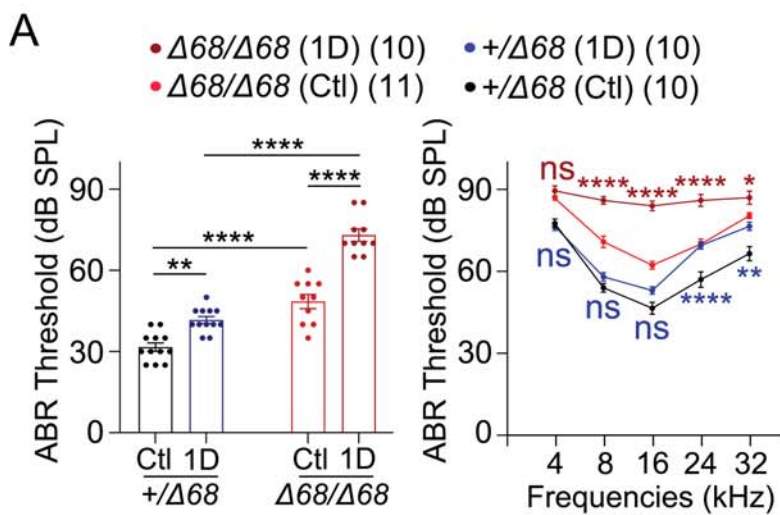


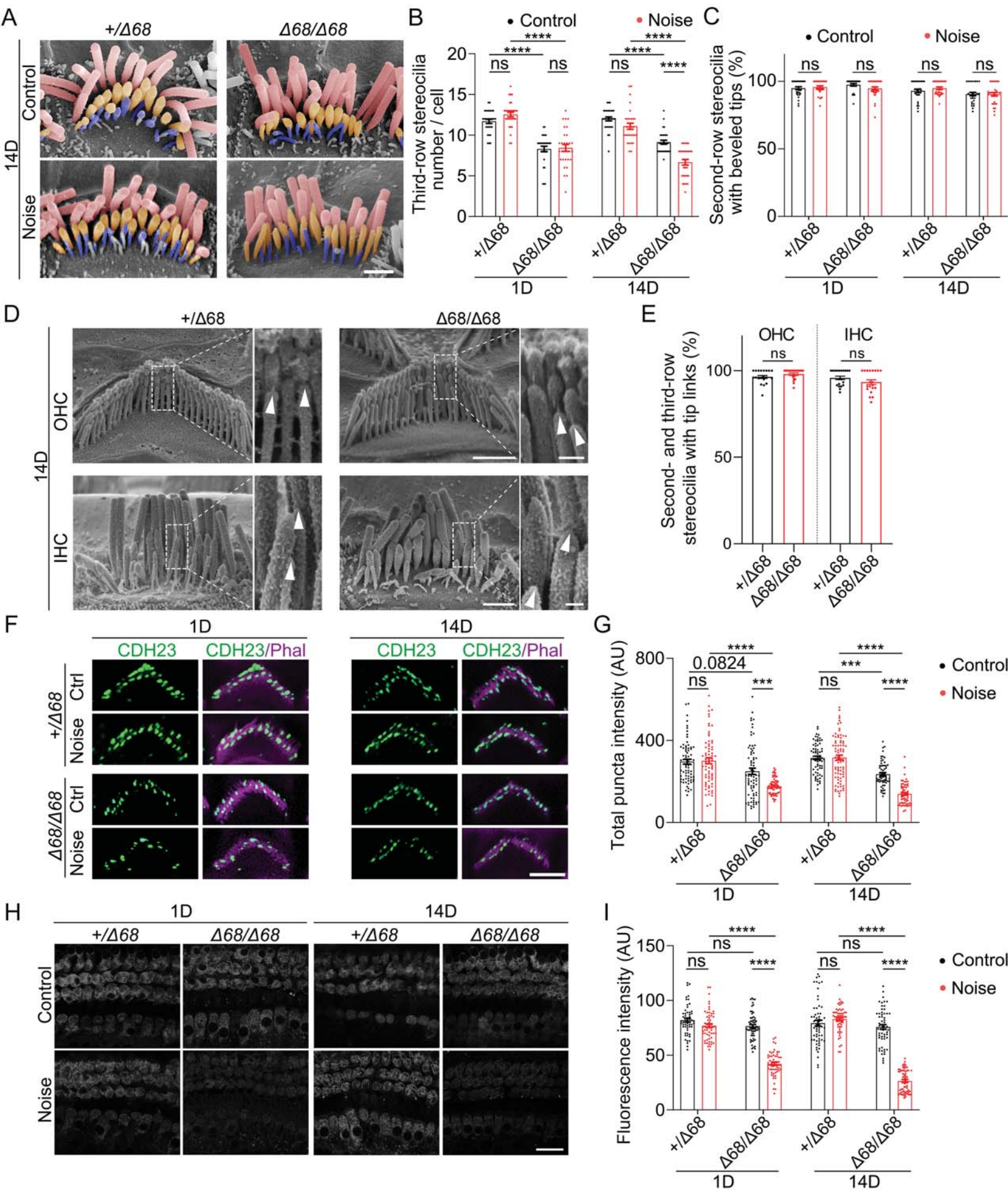




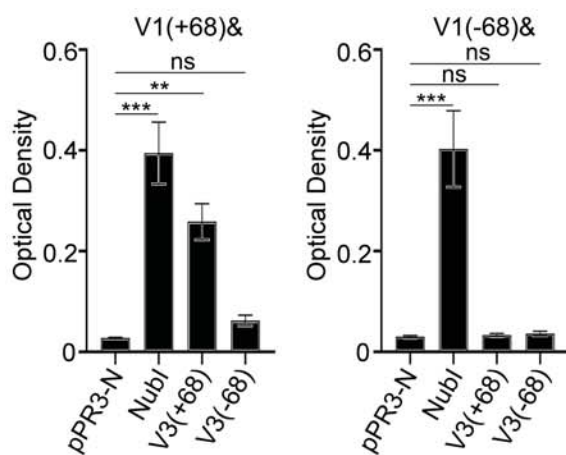
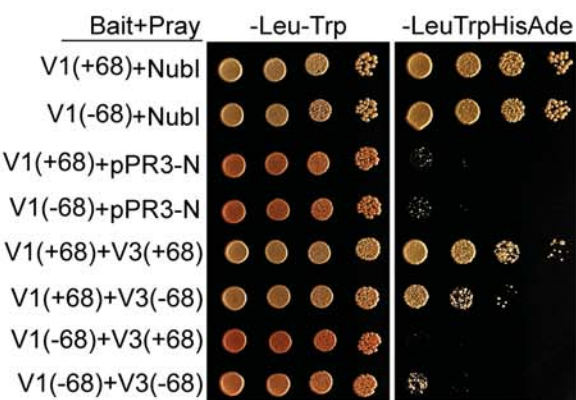




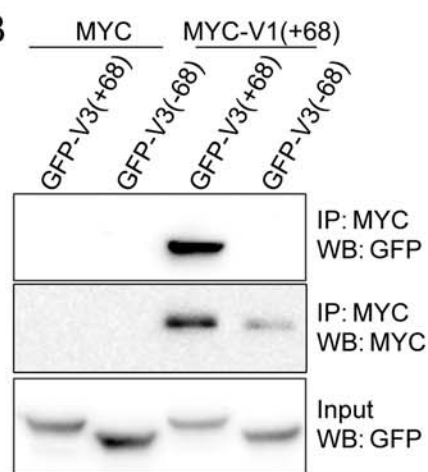




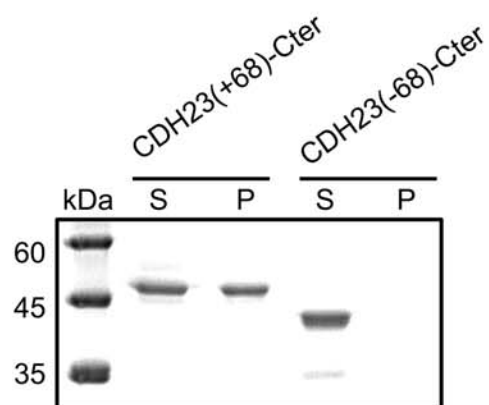
A



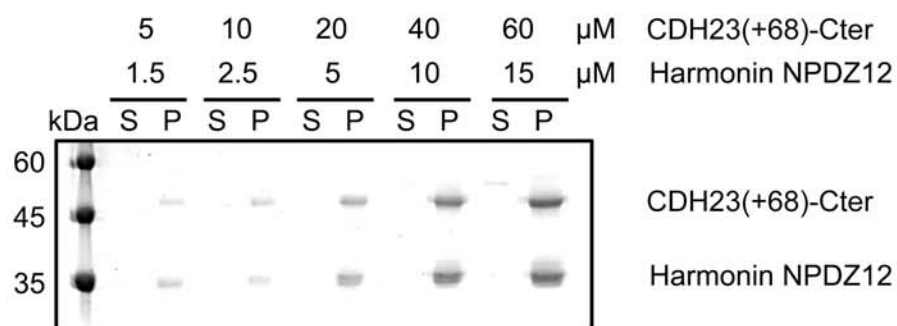
B



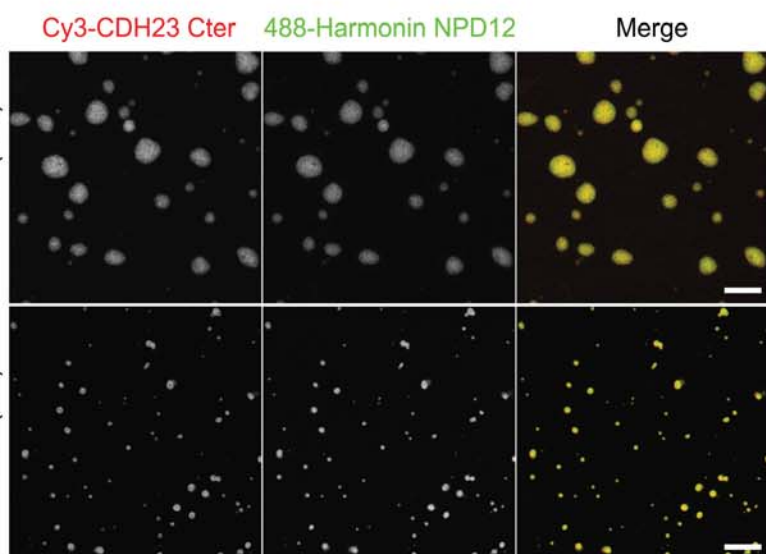
C



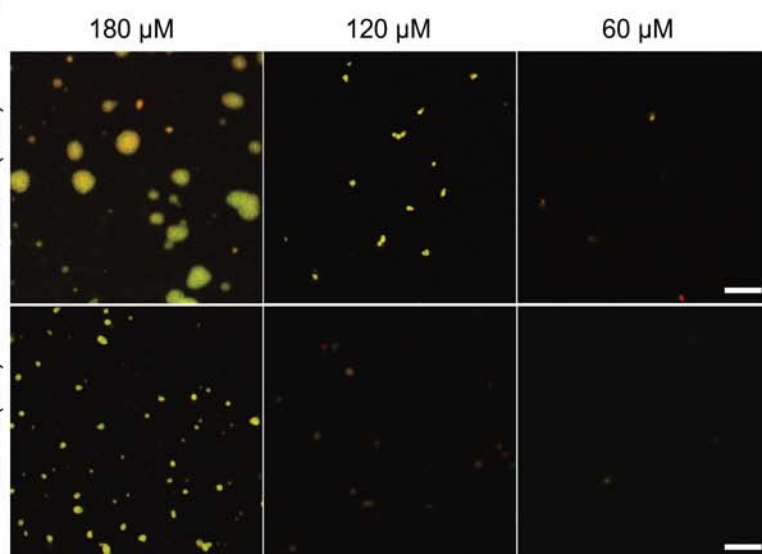
D



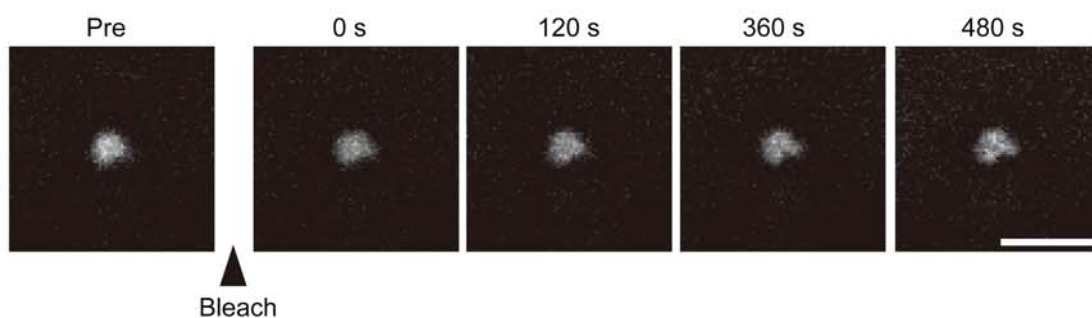
E



F



G



H

